^{210}Po and ^{210}Pb distributions during a phytoplankton bloom in the North Atlantic: Implications for POC export

Evan J. Horowitz [a], J. Kirk Cochran [a,*], Michael P. Bacon [b], David J. Hirschberg [a]

[a] School of Marine & Atmospheric Sciences, Stony Brook University, Stony Brook, NY, 11794, USA
[b] Woods Hole Oceanographic Institution, Woods Hole, MA, 02543, USA

A R T I C L E   I N F O

A B S T R A C T

During the North Atlantic Bloom Experiment (NABE) of the Joint Global Ocean Flux Study (JGOFS), water column sampling for particulate and dissolved ^{210}Po and ^{210}Pb was performed four times (26 April and 4, 20, 30 May 1989) during a month-long Lagrangian time-series occupation of the NABE site, as well as one-time samplings at stations during transit to and from the site. There are few prior studies documenting short-term changes in ^{210}Po and ^{210}Pb profiles over the course of a phytoplankton bloom, and we interpret the profiles in terms of the classical "steady-state" (SS) approach used in most studies, as well as by using a non-steady state approach suggested by the temporal evolution of the profiles. Changes in ^{210}Po profiles during a bloom are expectable as this radionuclide is scavenged and exported. During NABE, ^{210}Pb profiles also displayed non-steady state, with significant increases in upper water column inventory occurring midway through the experiment. Export of ^{210}Po from the upper 150 m using the classic "steady-state" model shows increases from 0.5 ± 8.5 dpm m^{-2} d^{-1} to 68.2 ± 4.2 dpm m^{-2} d^{-1} over the ~one-month occupation. Application of a non-steady state model, including changes in both ^{210}Pb and ^{210}Po profiles, gives higher ^{210}Po export fluxes. Detailed depth profiles of particulate organic carbon (>0.8 μm) and particulate ^{210}Po (>0.4 μm) are available from the 20 and 30 May samplings and show maxima in POC/Po at ~37 m. Applying the POC/^{210}Po ratios at 150 m to the "steady state" ^{210}Po fluxes yields POC export from the upper 150 m of 8.2 ± 1.5 mmol C m^{-2} d^{-1} on 20 May and 6.0 ± 1.6 mmol C m^{-2} d^{-1} on 30 May. The non-steady state model applied to the interval 20 to 30 May yields POC export of 24.3 mmol C m^{-2} d^{-1}. The non-steady state (NSS) ^{210}Po-derived POC fluxes are comparable to, but somewhat less than, those estimated previously from ^{234}Th/^{238}U disequilibrium for the same time interval (37.3 and 45.0 mmol m^{-2} d^{-1}, depending on the POC/Th ratio used). In comparison, POC fluxes measured with a floating sediment trap deployed at 150 m from 20 to 30 May were 11.6 mmol m^{-2} d^{-1}. These results suggest that non-steady state Po-derived POC fluxes during the NABE agree well with those derived from ^{234}Th/^{238}U disequilibrium and agree with sediment trap fluxes within a factor of ~2. However, unlike the ^{234}Th-POC flux proxy, non-steady stage changes in profiles of ^{210}Pb, the precursor of ^{210}Po, must be considered.

1. Introduction

The North Atlantic Bloom Experiment (NABE), carried out in 1989 as part of the Joint Global Ocean Flux Study (JGOFS), was a collaborative effort involving over 200 researchers from more than a dozen countries on six research vessels of different national origins. Although there were many purposes of this study, one of the most important goals was to quantify the flux of particulate organic carbon (POC) from the surface to depth throughout the duration of the bloom as a means to describe the bloom's effect on carbon sequestration in the ocean. Two methods were

used to quantify the POC flux during the NABE: sediment traps (Martin et al., 1993) and ^{238}U–^{234}Th disequilbrium (Buesseler et al., 1992). Here we present previously unpublished ^{210}Pb and ^{210}Po data from samples collected during the NABE and use the disequilibrium between ^{210}Pb (half-life = 22.3 y) and its radioactive granddaughter ^{210}Po (half-life = 138.4 d) to calculate POC fluxes for comparison with the sediment trap and Th-derived estimates. Although the samples were collected and processed some time ago, their publication is relevant now because of the increased use of the ^{210}Pb-^{210}Po proxy to estimate POC flux (e.g. Tang et al., 2019; Hayes et al., 2018). The data set is one among

---

only a few Lagrangian time-series data sets of ^{210}Po-^{210}Pb (Kim and Church, 2001; Friedrich and Rutgers van der Loeff, 2002; Stewart et al., 2007, 2011) and is the only one to sample extensively during a phytoplankton bloom. Moreover, although the preferential scavenging of ^{210}Po relative to ^{210}Pb had been well documented in GEOSECS and other studies prior to the NABE (Cochran et al., 1983; Bacon et al., 1976, 1988), as had the tendency of Po to concentrate in organic particles (Cherry and Heyraud, 1981), the disequilibrium between ^{210}Po and ^{210}Pb was seldom viewed in the context of a link to primary production or POC export, as in more recent applications.

Both of the radionuclide pairs, ^{238}U–^{234}Th and ^{210}Pb-^{210}Po, occur in the naturally-occurring ^{238}U decay series and both can display disequilibrium in ocean profiles. The disequilibrium between ^{238}U and

^{234}Th in the ocean was first described by Bhat et al. (1968) and arises from the particle reactive nature of Th. Indeed, thorium has a distribution coefficient (K_d) of ~10^6–10^7, making it one of the strongest particle-reactive elements (IAEA, 1985). Uranium primarily exists in the form of $UO_2(CO_3)_3^{4-}$ in ambient seawater (Endrizzi and Rao, 2014), and because particles in the ocean also tend to have a negative charge, uranium is not adsorbed to them. Therefore, uranium is effectively conservative in the ocean, and its concentration at any site can be calculated through a simple relationship to salinity (Chen et al., 1986). A fraction of the ^{234}Th ($t_{1/2} = 24$ d) that is produced from decay of ^{238}U ($t_{1/2} = 4.5 \times 10^9$ years) can be adsorbed onto sinking particles and transported downwards, resulting in a ^{234}Th deficit that can be converted to a POC flux if the POC/^{234}Th ratio on the sinking particles is
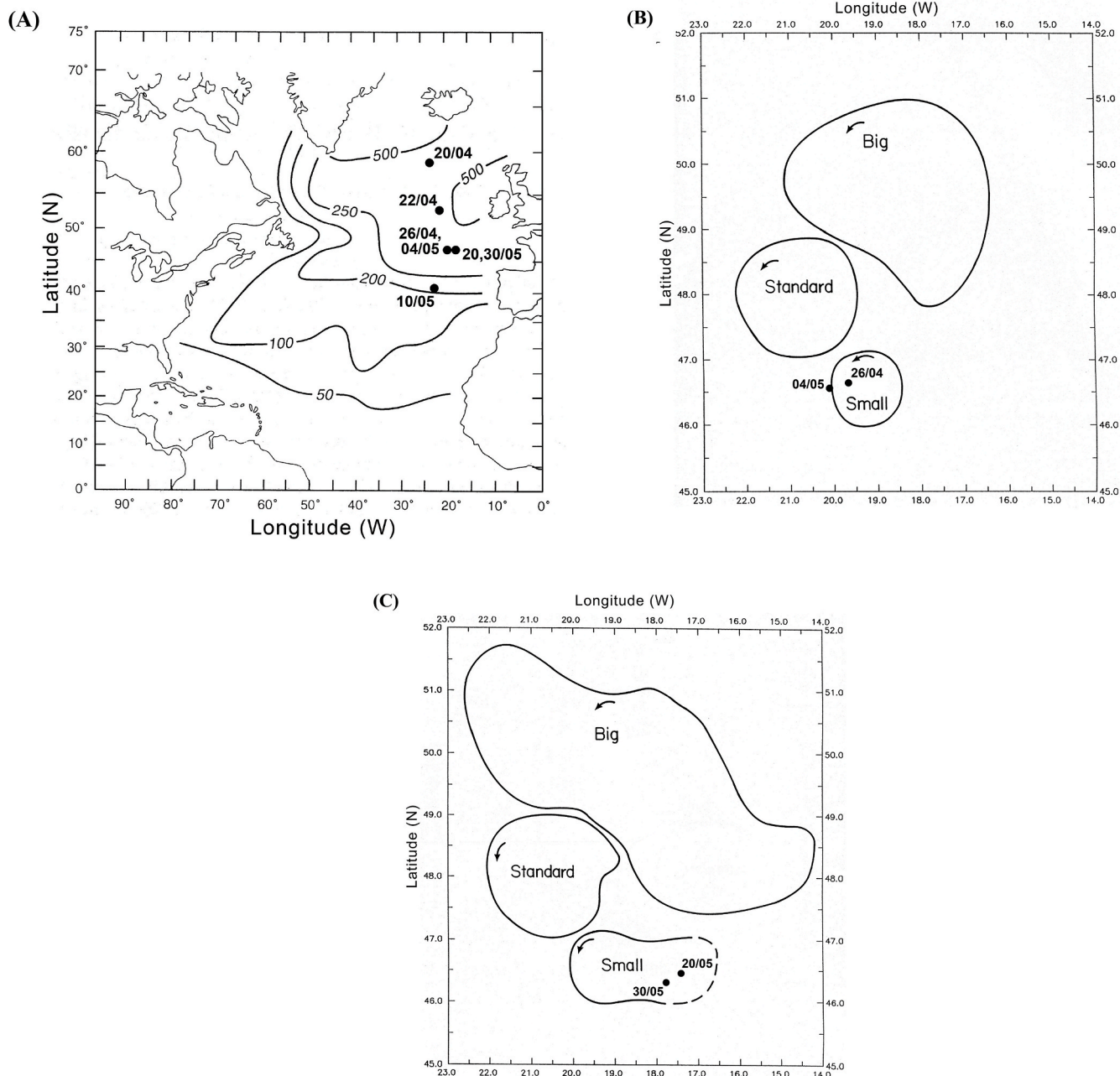

Fig. 1. (A) Locations and dates of stations where ^{210}Pb and ^{210}Po measurement occurred during the JGOFS North Atlantic Bloom Experiment (NABE) in 1989. Stations are labeled with date sampled (as dd/mm). Stations on 26/04, 04, 20 and 30/05 represent the NABE time series stations. Contours represent winter mixed layer depth. Modified from Ducklow and Harris (1993). (B) Location of stations on 26/04 and 04/05 relative to eddy field in the sampling area. (C) Location of stations on 20/05 and 30/05 relative to eddy field in the sampling area. Note eastward extension and partial breakdown of eddy "Small". Modified from Slagle and Heimerdinger (1991) and Robinson et al. (1993).

known. The ^{210}Po-POC flux proxy works in a similar manner, but its grandparent, ^{210}Pb, is not conservative, and can also be scavenged from the water column. ^{210}Pb is added to the surface ocean by atmospheric deposition (via decay of ^{222}Rn through several short-lived isotopes) and is also produced throughout the water column by ^{226}Ra decay. ^{210}Pb decays to ^{210}Po via the short-lived ^{210}Bi ($t_{1/2}$ = 5.0 days). Po is scavenged by organic matter more efficiently than Pb (Tang et al., 2017), due to its assimilation into proteins, likely as an analogue of sulfur (Stewart and Fisher, 2003). A significant fraction (40–50%) of sinking particulate organic matter (POM) is composed of amino acids (Hedges et al., 2001), suggesting that sinking POM is a major pathway for removal of ^{210}Po from the euphotic zone. Previous work has shown that ^{210}Po is removed from the upper water column more rapidly than ^{210}Pb, causing a deficiency of ^{210}Po relative to ^{210}Pb (Bacon et al., 1976; Nozaki et al., 1996). This deficit, together with the measured ratio of POC to ^{210}Po on sinking particles can be used to calculate a POC flux in the upper water column in a manner similar to the ^{234}Th-POC flux proxy (Cochran and Masqué, 2003). At depth, ^{210}Po can be released from sinking organic matter by remineralization, creating an excess in the mesopelagic zone (Cochran et al., 1983; Bacon et al., 1988). Because the ^{210}Po deficit is maintained with a different mechanism than the ^{234}Th deficit (assimilation and scavenging vs. only scavenging), and the two radionuclides have different half-lives (138.4 days for ^{210}Po vs. 24.1 days for ^{234}Th), comparison between the two POC flux proxies may impart additional knowledge about the system, and constrain the time window during which POC export may have occurred (Stewart et al., 2007).

2. Sampling and methods

Sampling for ^{210}Pb and ^{210}Po took place at seven stations during the ~2 months duration of the NABE (Fig. 1A). We report data collected during the US JGOFS NABE cruise on the R/V *Atlantis II* in 1989. A Lagrangian time-series site was established with repeated sampling in the vicinity of 46°N, 20°W. The site was in deep water, ~4560 m (Pfannkuche, 1993). The cruise initiated in Iceland and was divided into two legs (Leg 1: 17 April – 11 May and Leg 2: 15 May to 6 June 1989) with a port stop in the Azores between the legs. Sampling at the NABE site was designed to follow drifting buoys, including a 1500 m-deep drifting sediment trap array (Martin et al., 1993). Additionally, Robinson et al. (1993) used real-time remote sensing to document the presence of three eddies in the NABE area, and attempts were made to confine sampling to one eddy (designated "Small"). Fig. 1 (B and C) shows how sampling sites shifted over time, consistent with tracking buoys and positioning with eddy "Small".

In addition to the time-series sampling at the NABE site, two stations were taken during transit of the ship from Iceland to the NABE site (20, 22 April) and one during transit to the cruise changeover in the Azores (10 May). ^{210}Pb and ^{210}Po activity profiles were measured at the transit stations and at the NABE site over ~1 month on 26 April, and 4, 20 and 30 May. For comparison with other estimates of POC flux at NABE, we focus here primarily on these four time-series profiles of ^{210}Po and ^{210}Pb.

Water samples (~14–20L) were taken for ^{210}Po and ^{210}Pb analysis by rosette sampler in the upper water column (to 500–1500 m). Samples were filtered through 47-mm diameter 0.4 μm Nucleopore™ filters to collect particulate ^{210}Po and ^{210}Pb and the filtered water was then acidified to pH ~1.7 with HCl. ^{209}Po tracer and stable Pb carrier were added and the samples were allowed to equilibrate for ~24 h. A solution of ammonium pyrolidine dithiocarbamate (APDC) was added to the sample to chelate Po and Pb, and then ^{210}Po and ^{210}Pb were concentrated by flocculating the colloidal chelate through addition of excess cobalt, as Co(NO$_3$)$_2$, to the sample (Co-APDC; Fleer and Bacon, 1984; Chung et al., 1983; Cochran et al., 1983). The Co-APDC precipitate was filtered onto 142-mm diameter 0.45 μm Millipore™ filters. The filters containing the Co-APDC precipitates and particles were returned to the laboratories (Stony Brook and Woods Hole) promptly after each leg for processing.

In the laboratory, the filters containing the Co-APDC were dissolved in a mixture of HNO$_3$ and HClO$_4$. Following evaporation, the samples were picked up in 1.5N HCl, and Po was plated onto silver disks (Flynn, 1968). The disks were mounted in specially designed Teflon holders with an embedded magnet. Plating proceeded by heating the samples on a magnetic stirrer hot plate at 80 °C for 3–4 h. The rotation of the Teflon holders served to stir the solution and enhanced its contact with the planchet. The particulate filters were totally dissolved in a mixture of HF, HNO$_3$ and HCl and evaporated to dryness several times to ensure that the sample was in the Cl$^-$ form. It was then picked up in 1.5N HCl for plating of Po onto silver disks. Alpha activities of ^{210}Po and ^{209}Po were determined by counting with silicon surface barrier detectors using a Canberrra Quad Alpha system. Count rates were corrected for detector backgrounds and converted to activities based on the known activity of ^{209}Po tracer added. After determination of ^{210}Pb through additional Po ingrowth, the initial ^{210}Po activities were corrected to the time of collection, taking into account Po decay and ingrowth from ^{210}Pb from collection to initial plating.

The Pb fractions were purified by ion exchange, additional ^{209}Po tracer was added, and the solutions were stored for ingrowth of ^{210}Po for determination of the ^{210}Pb activity. After ~6 months, Po was again plated onto silver disks. ^{210}Pb activities were determined from the ingrowth of ^{210}Po from the time of Pb purification and corrected for decay to the time of collection. Pb yields were determined by atomic absorption spectrophotometry measurement of the concentration of the Pb carrier in the final purified Pb fraction. Reagent blanks and detector backgrounds were taken into account in the calculation of activities. Errors represent 1σ uncertainties derived from counting statistics.

3. Results

Locations of all stations sampled are shown in Fig. 1A, and details of the locations of the time-series stations on the two legs are shown in Fig. 1B and C. Decay-corrected particulate, and dissolved ^{210}Pb and ^{210}Po activities for the time-series station are given in Table 1 and transit station activities are given in Table 2. Total activities were calculated by summing the activities of the two fractions, with propagation of errors. Time-series profiles of total ^{210}Pb and ^{210}Po in the upper 500 m at the NABE site are shown in Fig. 2. For the time-series station profiles, ^{210}Po minima were approximately coincident with the bottom of the mixed layer at each date (~100 m on 26/04, shoaling to 10–20 m thereafter; see section 4.1), and maxima occurred below 100m. Low near-surface activities and higher deep activities suggest transport of ^{210}Po from the upper to deep ocean. ^{210}Pb minima generally occurred deeper in the water column and maxima were observed in the upper 100m. This decrease in ^{210}Pb activity with depth suggests a surface source of ^{210}Pb, as indicated by ^{210}Pb activities greater than those of ^{226}Ra in the upper water column. The particulate ^{210}Po and ^{210}Pb data showed an excess of particulate ^{210}Po relative to ^{210}Pb, with ^{210}Po/^{210}Pb activity ratios often »1 (Table 1).

Profiles of dissolved and particulate ^{210}Po and ^{210}Pb from all stations are also shown in Supplemental Fig. S2. Particulate activities of both ^{210}Po and ^{210}Pb decreased with depth. At the time-series site (Supplemental Fig. S2- C, D, F G), dissolved ^{210}Pb activities were relatively constant with depth while dissolved ^{210}Po activities increased with depth, presumably due to rapid scavenging/assimilation of ^{210}Po near the surface and remineralization of particulate ^{210}Po at depth. Particulate ^{210}Pb was generally <10% of the total ^{210}Pb activity at all depths (Table 1). In contrast, in the upper ~20–100 m (corresponding to the mixed layer; see section 4.1) particulate ^{210}Po often exceeded the dissolved ^{210}Po and dominated the total ^{210}Po. The ^{210}Po/^{210}Pb activity ratios in the dissolved, particulate, and total fractions at the time-series station (Table 1) reinforce the notion that it is mostly ^{210}Po rather than ^{210}Pb that is being transported downwards by particles, as almost all particulate ^{210}Po/^{210}Pb ratios were much greater than one, especially in the upper ~500m of the water column. The dissolved ^{210}Po/^{210}Pb ratios

Table 1

^{210}Po and ^{210}Pb data from NABE Time Series Stations*.

Date and station identifiers	Depth (m)	$^{210}Pb_d$ (dpm/ 100kg)	$^{210}Pb_p$ (dpm/ 100kg)	$^{210}Pb_t$ (dpm/ 100kg)	$^{210}Po_d$ (dpm/ 100kg)	$^{210}Po_p$ (dpm/ 100kg)	$^{210}Po_t$ (dpm/ 100kg)	$^{210}Po_d/^{210}Pb_d$	$^{210}Po_p/^{210}Pb_p$	$^{210}Po_t/^{210}Pb_t$
26 April	**29**	10.9 ± 0.3	0.5 ± 0.1	11.4 ± 0.3	5.9 ± 0.8	5.0 ± 0.3	10.9 ± 0.9	0.5 ± 0.1	10.0 ± 2.1	1.0 ± 0.1
	53	9.3 ± 0.6	0.6 ± 0.1	9.9 ± 0.6	8.6 ± 0.9	3.1 ± 0.6	11.7 ± 1.1	0.9 ± 0.1	5.2 ± 1.3	1.2 ± 0.1
S11–C9	**77**	10.6 ± 0.5	ND	ND	3.9 ± 0.2	5.5 ± 0.8	9.4 ± 0.8	0.5 ± 0.1	ND	ND
46°42.5′N	**102**	8.7 ± 2.1	0.5 ± 0.1	9.2 ± 2.1	5.4 ± 1.5	3.3 ± 0.5	8.7 ± 1.6	0.6 ± 0.2	6.6 ± 1.7	0.9 ± 0.3
19°44.1′W	**196**	9.6 ± 0.6	0.5 ± 0.2	10.1 ± 0.6	9.0 ± 0.6	1.9 ± 0.2	10.9 ± 0.6	0.9 ± 0.1	3.8 ± 1.6	1.1 ± 0.1
	300	11.4 ± 0.7	0.3 ± 0.1	11.7 ± 0.7	9.8 ± 0.7	1.0 ± 0.1	10.8 ± 0.7	0.9 ± 0.1	3.3 ± 1.2	0.9 ± 0.1
	407	10.9 ± 0.7	0.1 ± 0.1	11.0 ± 0.7	11.4 ± 0.6	1.7 ± 0.2	13.1 ± 0.6	1.0 ± 0.1	17.0 ± 17.1	1.2 ± 0.1
	501	11.6 ± 1.1	0.2 ± 0.1	11.8 ± 1.1	12.1 ± 0.6	1.7 ± 0.1	13.8 ± 0.6	1.0 ± 0.1	8.5 ± 4.3	1.2 ± 0.1
	599	10.9 ± 0.7	0.1 ± 0.1	11.0 ± 0.7	9.2 ± 1.0	0.5 ± 0.1	9.7 ± 1.0	0.8 ± 0.1	5.0 ± 5.1	0.9 ± 0.1
	1046	7.4 ± 0.6	0.3 ± 0.1	7.7 ± 0.6	6.3 ± 0.4	1.2 ± 0.1	7.5 ± 0.4	0.9 ± 0.1	4.0 ± 1.4	1.0 ± 0.1
	1542	8.5 ± 0.6	0.1 ± 0.1	8.6 ± 0.6	6.6 ± 0.4	1.1 ± 0.1	7.7 ± 0.4	0.8 ± 0.1	11.0 ± 11.0	0.9 ± 0.1
	1972	6.5 ± 0.7	0.2 ± 0.1	6.7 ± 0.7	5.9 ± 0.4	0.1 ± 0.1	6.0 ± 0.4	0.9 ± 0.1	0.5 ± 0.6	0.9 ± 0.1
4 May	**0**	11.9 ± 0.5	1.3 ± 0.1	13.2 ± 0.5	3.5 ± 0.6	7.0 ± 0.3	11.1 ± 0.7	0.3 ± 0.1	5.4 ± 0.5	0.8 ± 0.1
	20	11.1 ± 0.4	1.1 ± 0.1	12.1 ± 0.4	4.5 ± 0.7	4.5 ± 0.2	9.0 ± 0.7	0.4 ± 0.1	4.1 ± 0.4	0.7 ± 0.1
S19–C7	**50**	11.9 ± 0.4	0.6 ± 0.2	12.5 ± 0.5	6.7 ± 0.7	4.1 ± 0.2	10.8 ± 0.7	0.6 ± 0.1	6.8 ± 2.3	0.9 ± 0.1
46°40.0′N	**75**	11.8 ± 0.6	0.1 ± 0.1	11.9 ± 0.6	9.8 ± 0.8	2.4 ± 0.1	12.2 ± 0.8	0.8 ± 0.1	24.0 ± 24.0	1.0 ± 0.1
20°10.2′W	**100**	11.9 ± 0.4	0.7 ± 0.1	12.6 ± 0.4	9.2 ± 0.7	2.1 ± 0.2	11.3 ± 0.7	0.9 ± 0.1	3.0 ± 0.5	0.9 ± 0.1
	150	10.6 ± 0.4	0.2 ± 0.1	10.8 ± 0.4	12.9 ± 0.9	1.7 ± 0.1	14.6 ± 0.9	1.2 ± 0.1	8.5 ± 4.3	1.4 ± 0.1
	200	10.7 ± 0.4	0.5 ± 0.1	11.2 ± 0.3	10.9 ± 0.9	ND	ND	1.0 ± 0.1	ND	ND
	300	9.6 ± 0.3	0.4 ± 0.1	10.0 ± 0.3	9.2 ± 0.7	1.6 ± 0.1	10.8 ± 0.7	1.0 ± 0.1	4.0 ± 1.0	1.1 ± 0.1
	400	9.8 ± 0.3	0.2 ± 0.1	10.0 ± 0.3	13.1 ± 0.8	0.9 ± 0.1	14.0 ± 0.8	1.3 ± 0.1	4.5 ± 2.3	1.4 ± 0.1
	600	9.1 ± 0.4	0.2 ± 0.1	9.3 ± 0.5	11.2 ± 0.7	1.3 ± 0.1	12.5 ± 0.7	1.2 ± 0.1	6.5 ± 3.3	1.3 ± 0.1
	1050	7.0 ± 0.3	0.3 ± 0.1	7.2 ± 0.3	8.9 ± 0.7	ND	ND	1.3 ± 0.1	ND	ND
	1550	10.9 ± 0.3	0.3 ± 0.1	11.4 ± 0.3	5.9 ± 0.8	5.0 ± 0.3	10.9 ± 0.9	0.5 ± 0.1	16.7 ± 5.6	1.0 ± 0.1
20 May	**4**	16.6 ± 0.8	2.1 ± 0.1	18.7 ± 0.8	2.2 ± 0.7	5.3 ± 0.2	7.6 ± 0.7	0.1 ± 0.04	2.5 ± 0.2	0.4 ± 0.04
	7	16.4 ± 0.6	1.5 ± 0.1	17.8 ± 0.6	3.3 ± 0.6	4.9 ± 0.2	8.2 ± 0.6	0.2 ± 0.04	3.3 ± 0.3	0.5 ± 0.04
S27–C1	**22**	15.4 ± 0.7	1.2 ± 0.1	16.7 ± 0.7	3.1 ± 0.8	3.4 ± 0.2	6.6 ± 0.8	0.2 ± 0.05	2.8 ± 0.3	0.4 ± 0.1
46°31.7′N	**37**	ND	0.9 ± 0.1	ND	ND	2.3 ± 0.2	ND	ND	2.6 ± 0.4	ND
17°41.1.'W	**52**	ND	0.5 ± 0.0	ND	ND	2.3 ± 0.2	ND	ND	4.6 ± 0.4	ND
	77	20.4 ± 0.7	0.3 ± 0.03	20.7 ± 0.7	7.9 ± 1.0	1.4 ± 0.2	9.3 ± 1.0	0.4 ± 0.1	4.7 ± 0.8	0.4 ± 0.1
	102	16.9 ± 0.8	1.1 ± 0.1	18.1 ± 0.8	9.2 ± 1.0	2.0 ± 0.2	11.2 ± 1.0	0.6 ± 0.1	1.8 ± 0.2	0.6 ± 0.1
	151	15.4 ± 0.7	0.3 ± 0.03	15.7 ± 0.7	8.3 ± 1.0	1.1 ± 0.2	9.3 ± 1.0	0.5 ± 0.1	3.7 ± 0.8	0.6 ± 0.1
	201	15.4 ± 0.8	0.3 ± 0.23	15.6 ± 0.8	10.3 ± 0.9	1.4 ± 0.1	11.6 ± 0.9	0.7 ± 0.1	4.7 ± 3.6	0.7 ± 0.1
	299	14.9 ± 0.7	0.4 ± 0.03	15.3 ± 0.7	9.6 ± 1.0	1.6 ± 0.1	11.2 ± 1.0	0.7 ± 0.1	4.0 ± 0.4	0.7 ± 0.1
	396	14.9 ± 0.6	0.2 ± 0.02	15.1 ± 0.6	8.6 ± 1.2	1.1 ± 0.1	9.7 ± 1.2	0.6 ± 0.1	5.5 ± 0.7	0.6 ± 0.1
	493	13.0 ± 0.6	0.3 ± 0.02	13.3 ± 0.6	8.9 ± 0.5	1.3 ± 0.1	10.2 ± 0.5	0.7 ± 0.1	4.3 ± 0.4	0.8 ± 0.1
30 May	**4**	14.0 ± 0.6	2.0 ± 0.1	15.9 ± 0.6	1.4 ± 0.7	5.7 ± 0.2	7.1 ± 0.7	0.1 ± 0.5	2.9 ± 0.2	0.4 ± 0.1
	7	15.3 ± 0.8	2.4 ± 0.1	17.7 ± 0.8	0.6 ± 0.6	6.1 ± 0.2	6.7 ± 0.6	0.03 ± 0.03	2.5 ± 0.1	0.4 ± 0.04
S37–C8	**23**	13.4 ± 0.6	2.1 ± 0.1	15.6 ± 0.6	2.8 ± 0.5	4.1 ± 0.2	6.9 ± 0.5	0.2 ± 0.2	2.0 ± 0.1	0.4 ± 0.04
46°22.3′N	**38**	14.9 ± 0.7	1.0 ± 0.1	15.9 ± 0.7	2.8 ± 0.6	2.0 ± 0.2	4.8 ± 0.7	0.2 ± 0.2	2.0 ± 0.3	0.3 ± 0.1
17°51.5′W	**52**	13.6 ± 0.8	0.6 ± 0.1	14.2 ± 0.8	5.2 ± 0.6	1.5 ± 0.1	6.7 ± 0.6	0.4 ± 0.1	2.5 ± 0.4	0.5 ± 0.1
	77	14.5 ± 0.6	0.3 ± 0.0	14.8 ± 0.6	7.5 ± 0.7	1.1 ± 0.1	8.6 ± 0.7	0.5 ± 0.1	3.7 ± 0.3	0.6 ± 0.1
	102	13.7 ± 0.6	0.2 ± 0.0	13.9 ± 0.6	8.8 ± 0.7	1.0 ± 0.1	9.8 ± 0.7	0.6 ± 0.1	5.0 ± 0.5	0.7 ± 0.1
	152	14.4 ± 0.6	ND	ND	8.4 ± 0.6	ND	ND	0.6 ± 0.1	ND	ND
	202	13.7 ± 0.6	0.3 ± 0.0	13.9 ± 0.6	8.9 ± 0.7	1.0 ± 0.1	9.9 ± 0.7	0.7 ± 0.1	3.3 ± 0.3	0.7 ± 0.1
	301	13.7 ± 0.5	0.3 ± 0.0	14.1 ± 0.5	7.6 ± 0.7	0.7 ± 0.1	8.3 ± 0.7	0.6 ± 0.1	2.3 ± 0.3	0.6 ± 0.1
	400	13.6 ± 0.5	0.1 ± 0.0	13.7 ± 0.5	9.5 ± 0.7	1.2 ± 0.1	10.8 ± 0.7	0.7 ± 0.1	12.0 ± 1.0	0.8 ± 0.1
	499	12.9 ± 0.6	0.3 ± 0.0	13.2 ± 0.6	6.6 ± 0.7	0.9 ± 0.1	7.5 ± 0.7	0.5 ± 0.1	3.0 ± 0.3	0.6 ± 0.1

*d, p and t subscripts represent dissolved, particulate and total activities. ND = No Data.

complemented the elevated particulate ^{210}Po/^{210}Pb, with values < 1.0 at the surface, increasing toward 1 with depth as the particulate fraction of each radionuclide decreased relative to the total.

Profiles of total ^{210}Po and ^{210}Pb activities were integrated to depths of 150 and 300 m using trapezoidal integration. ^{210}Pb inventories in the upper 300 m increased over the course of the study, with a noticeable increase occurring between the sampling on 4 May and 20 May at the NABE site (Table 3; Fig. 3). ^{210}Po deficits also increased over the course of the bloom time series and, as with the ^{210}Pb inventories, increased markedly between the 4 May and 20 May samplings (Table 3, Fig. 3). The profiles of total ^{210}Pb and ^{210}Po at the transit stations are given in Supplemental Fig. S1. Upper water column ^{210}Po deficits were evident in the more northern stations on 20 and 22 April and were higher than the

deficits on 26 April at the times-series site, suggesting that the bloom commenced earlier north of the time-series stations (Tables 3 and 4). In contrast, the lack of a significant ^{210}Po deficit south of the time-series station on 10 May (Table 4; Supplemental Fig. S1C) indicated low Po export, due either to lower productivity south of the time-series location or a later initiation of the bloom at that location.

4. Discussion

4.1. Hydrographic influences

Hydrographic data (water column salinity and temperature; Fig. 4) for the four dates of the time-series study indicate that the water column

Table 2
^{210}Po and ^{210}Pb data from NABE Transit Stations*.

Date and station identifiers	Depth (m)	^{210}Pb$_d$ (dpm/ 100kg)	^{210}Pb$_p$ (dpm/ 100kg)	^{210}Pb$_t$ (dpm/ 100kg)	^{210}Po$_d$ (dpm/ 100kg)	^{210}Po$_p$ (dpm/ 100kg)	^{210}Po$_t$ (dpm/ 100kg)	^{210}Po$_d$/^{210}Pb$_d$ (dpm/100kg)	^{210}Po$_p$/^{210}Pb$_p$ (dpm/100kg)	^{210}Po$_t$/^{210}Pb$_t$ (dpm/100kg)
20 April	28	9.9 ± 0.4	0.4 ± 0.1	10.3 ± 0.4	9.0 ± 0.3	1.1 ± 0.1	10.1 ± 0.3	0.9 ± 0.1	2.8 ± 0.7	1.0 ± 0.1
	53	11.0 ± 0.6	2.5 ± 1.6	13.5 ± 1.7	9.3 ± 0.4	0.8 ± 0.2	10.2 ± 0.4	0.9 ± 0.1	0.3 ± 0.2	0.8 ± 0.1
S4–C2	78	10.6 ± 0.5	0.7 ± 0.1	11.3 ± 0.5	8.4 ± 0.3	1.1 ± 0.2	9.5 ± 0.4	0.8 ± 0.1	1.6 ± 0.4	0.8 ± 0.1
59°45.8′N	103	11.7 ± 0.6	0.3 ± 0.1	11.9 ± 0.6	8.1 ± 0.3	0.8 ± 0.1	8.9 ± 0.3	0.7 ± 0.1	2.7 ± 0.9	0.7 ± 0.1
20°38.6′W	152	10.5 ± 0.6	0.6 ± 0.2	11.2 ± 0.7	8.0 ± 0.4	1.1 ± 0.2	9.1 ± 0.4	0.8 ± 0.1	1.8 ± 0.7	0.8 ± 0.1
	201	8.8 ± 0.6	0.4 ± 0.1	9.3 ± 0.6	8.3 ± 0.4	0.7 ± 0.1	9.1 ± 0.4	0.9 ± 0.1	1.8 ± 0.5	1.0 ± 0.1
	299	ND	ND	ND	8.6 ± 0.4	0.7 ± 0.1	9.3 ± 0.4	ND	ND	ND
	395	9.4 ± 0.4	0.2 ± 0.1	9.6 ± 0.4	7.2 ± 0.5	0.6 ± 0.1	7.8 ± 0.5	0.8 ± 0.1	3.0 ± 1.6	0.8 ± 0.1
	499	7.3 ± 0.4	1.0 ± 0.2	8.3 ± 0.4	8.9 ± 0.7	0.4 ± 0.1	9.3 ± 0.7	1.2 ± 0.1	0.4 ± 0.1	1.1 ± 0.1
	953	7.1 ± 0.4	0.1 ± 0.1	7.3 ± 0.4	6.5 ± 0.6	0.2 ± 0.1	6.7 ± 0.6	0.9 ± 0.1	2.0 ± 4.1	0.9 ± 0.1
	1131	6.2 ± 0.3	3.8 ± 0.3	9.9 ± 0.4	5.1 ± 0.4	3.6 ± 0.2	8.6 ± 0.4	0.8 ± 0.1	0.9 ± 0.1	0.9 ± 0.1
	1336	6.8 ± 0.5	1.0 ± 0.1	7.8 ± 0.5	7.9 ± 0.5	0.8 ± 0.1	8.7 ± 0.5	1.2 ± 0.1	0.8 ± 0.1	1.1 ± 0.1
22 April	27	12.8 ± 0.8	0.4 ± 0.1	13.2 ± 0.8	8.9 ± 0.3	1.1 ± 0.1	10.0 ± 0.3	0.7 ± 0.1	2.8 ± 0.7	0.8 ± 0.1
	52	12.0 ± 0.5	0.8 ± 0.1	12.7 ± 0.5	11.5 ± 0.4	0.7 ± 0.1	12.2 ± 0.4	1.0 ± 0.1	0.9 ± 0.2	1.0 ± 0.1
S7–C1	76	10.6 ± 0.5	0.3 ± 0.1	11.0 ± 0.5	8.8 ± 0.4	0.6 ± 0.1	9.5 ± 0.4	0.8 ± 0.1	2.0 ± 0.7	0.9 ± 0.1
53°30.3′N	100	10.6 ± 0.7	0.9 ± 0.1	11.6 ± 0.7	8.5 ± 0.2	0.6 ± 0.3	9.1 ± 0.4	0.8 ± 0.1	0.7 ± 0.3	0.8 ± 0.1
20°2.4′W	147	ND	0.2 ± 0.1	ND	8.5 ± 0.2	0.5 ± 0.1	9.0 ± 0.2	ND	2.5 ± 1.3	ND
	249	4.9 ± 0.3	6.3 ± 0.2	11.2 ± 0.4	4.6 ± 0.1	5.2 ± 0.2	9.9 ± 0.3	1.0 ± 0.1	0.8 ± 0.04	0.9 ± 0.04
	350	ND	0.8 ± 0.1	ND	6.7 ± 0.1	0.5 ± 0.1	7.2 ± 0.1	ND	0.6 ± 0.1	ND
	501	7.0 ± 0.8	0.8 ± 0.1	7.7 ± 0.8	5.0 ± 0.2	0.5 ± 0.1	5.4 ± 0.2	0.7 ± 0.1	0.6 ± 0.1	0.7 ± 0.1
	737	8.0 ± 0.6	0.0 ± 0.0	8.0 ± 0.6	6.8 ± 0.2	0.3 ± 0.1	7.1 ± 0.2	0.9 ± 0.1	ND	0.9 ± 0.1
	977	7.1 ± 0.4	1.0 ± 0.1	8.1 ± 0.4	5.8 ± 0.2	1.0 ± 0.1	6.9 ± 0.2	0.8 ± 0.1	1.0 ± 0.1	0.9 ± 0.1
	1164	7.2 ± 0.4	0.3 ± 0.1	7.5 ± 0.4	6.3 ± 0.2	0.4 ± 0.1	6.7 ± 0.2	0.9 ± 0.1	1.3 ± 0.6	0.9 ± 0.1
	1360	5.6 ± 0.3	0.6 ± 0.1	6.2 ± 0.3	7.5 ± 0.2	0.4 ± 0.1	7.9 ± 0.2	1.3 ± 0.1	0.7 ± 0.2	1.3 ± 0.1
10 May	13	ND	1.4 ± 0.2	ND	11.6 ± 0.5	2.1 ± 0.2	13.6 ± 0.5	ND	1.5 ± 0.3	ND
	43	ND	0.8 ± 0.3	ND	11.2 ± 0.5	1.4 ± 0.1	12.6 ± 0.5	ND	1.8 ± 0.7	ND
S24–C1	63	13.5 ± 0.5	0.6 ± 0.1	14.0 ± 0.5	12.4 ± 0.5	0.8 ± 0.1	13.2 ± 0.5	0.9 ± 0.1	1.3 ± 0.3	0.9 ± 0.1
41°5.8′N	82	13.6 ± 0.6	0.4 ± 0.2	14.0 ± 0.6	12.3 ± 0.4	0.5 ± 0.1	12.9 ± 0.4	0.9 ± 0.1	1.3 ± 0.7	0.9 ± 0.1
23°1.8′W	102	11.2 ± 0.4	0.4 ± 0.2	11.6 ± 0.4	12.2 ± 0.4	0.5 ± 0.1	12.7 ± 0.4	1.1 ± 0.0	1.3 ± 0.7	1.1 ± 0.1
	151	10.6 ± 0.8	0.4 ± 0.1	11.0 ± 0.8	11.7 ± 0.7	0.3 ± 0.1	11.9 ± 0.7	1.1 ± 0.1	0.8 ± 0.3	1.1 ± 0.1
	200	12.9 ± 0.5	0.2 ± 0.1	13.1 ± 0.5	12.6 ± 0.6	0.5 ± 0.1	13.1 ± 0.6	1.0 ± 0.1	2.5 ± 1.3	1.0 ± 0.1
	297	9.2 ± 0.5	0.6 ± 0.1	9.8 ± 0.5	11.7 ± 0.7	0.4 ± 0.1	12.1 ± 0.7	1.3 ± 0.1	0.7 ± 0.2	1.2 ± 0.1
	392	8.8 ± 0.4	0.2 ± 0.1	8.9 ± 0.4	10.2 ± 0.4	0.3 ± 0.1	10.6 ± 0.4	1.2 ± 0.1	1.5 ± 0.9	1.2 ± 0.1
	786	9.4 ± 0.4	1.0 ± 0.3	10.4 ± 0.5	8.3 ± 0.3	0.4 ± 0.1	8.7 ± 0.3	0.9 ± 0.1	0.4 ± 0.2	0.8 ± 0.1
	965	11.3 ± 1.4	0.6 ± 0.1	11.9 ± 1.4	7.8 ± 0.4	0.4 ± 0.1	8.2 ± 0.4	0.7 ± 0.1	0.7 ± 0.2	0.7 ± 0.1
	1457	8.4 ± 0.4	0.3 ± 0.1	8.6 ± 0.4	7.7 ± 0.3	0.5 ± 0.1	8.3 ± 0.3	0.9 ± 0.1	1.7 ± 0.6	1.0 ± 0.1

*d, p and t subscripts represent dissolved, particulate and total activities. ND = No Data.

was rapidly stratifying from summer heating, with a transition from a mixed layer of ~100 m on 26 April to ~20 m on 30 May. This shoaling of the mixed layer after winter deep convection supplies the surface with nutrients and is typically associated with the start of the spring bloom in the North Atlantic (Ducklow and Harris, 1993). Also, from the tracks of the free-floating buoys that were used to designate the NABE lagrangian time-series site and from satellite altimetry data, Robinson et al. (1993) determined that there was a field of three cyclonic (cold-core) eddies in the NABE sampling area, designated "Big," "Standard," and "Small" (Fig. 1B and C). Most NABE sampling on the R/V *Atlantis* took place within the "Small" eddy, which had a mean cyclonic surface current of 20 cm/s (Buesseler et al., 1992). During leg 1, the three eddies were well resolved (Fig. 1B), but distortion in the field was evident during leg 2 (Fig. 1C), and Robinson et al. (1993) described "another feature" interacting with the "Small" eddy. Indeed, Robinson et al. (1993) described providing "eddy reports" to the R/V *Atlantis* before each of the cruise legs, and noted that the "Small" eddy had moved eastward between the legs. Accordingly, sampling was adjusted eastward to remain within the eddy as the bloom time-series sampling continued (Fig. 1B vs 1C). In light of such a dynamic oceanographic regime, it remains difficult to maintain Lagrangian sampling of a single water mass over time, as noted by Lochte et al. (1993).

The "Small" eddy had rates of upwelling peaking at ~0.5 m/day (Robinson et al., 1993), and it is possible that this upwelling could have artificially lowered the ^{210}Po deficit by upwelling some dissolved ^{210}Po

from the deeper layers. However, enhanced production in these features seems to offset this effect. Indeed, Verdeny et al. (2008) found ^{210}Po fluxes and POC fluxes derived from the ^{210}Po-deficit that were moderately higher in cold-core eddies than outside them in the lee of the Hawaiian Islands. This conclusion suggests that the ^{210}Po flux and POC export calculated in the NABE eddy may not be completely representative of the larger region during the spring bloom. Although cold-core eddies do appear to have increased POC export compared to their surroundings, Verdeny et al. (2008) noted that the phytoplankton community structure, zooplankton grazing, and bacterial remineralization are the main influences on the POC export in a region. In the sections that follow, we calculate a steady state ^{210}Po flux, then discuss vertical advection and apply a non-steady-state model to calculate the ^{210}Po flux from the ^{210}Po deficit. The ^{210}Po flux and the ratio of POC/^{210}Po$_p$ are then used to calculate a POC flux on the two dates where the POC/^{210}Po$_p$ ratio could be determined (20 and 30 May).

4.2. ^{210}Pb-^{226}Ra disequilibrium

As noted above, ^{210}Pb, the grandparent of ^{210}Po, is not conservative and can be scavenged onto sinking particles. ^{210}Pb profiles from the NABE time series varied over the course of the bloom. Although no ^{226}Ra measurements were made during the NABE, earlier GEOSECS measurements (Broecker et al., 1976) showed relatively little variation in ^{226}Ra in the upper ~500 m of the water column in the North Atlantic. A
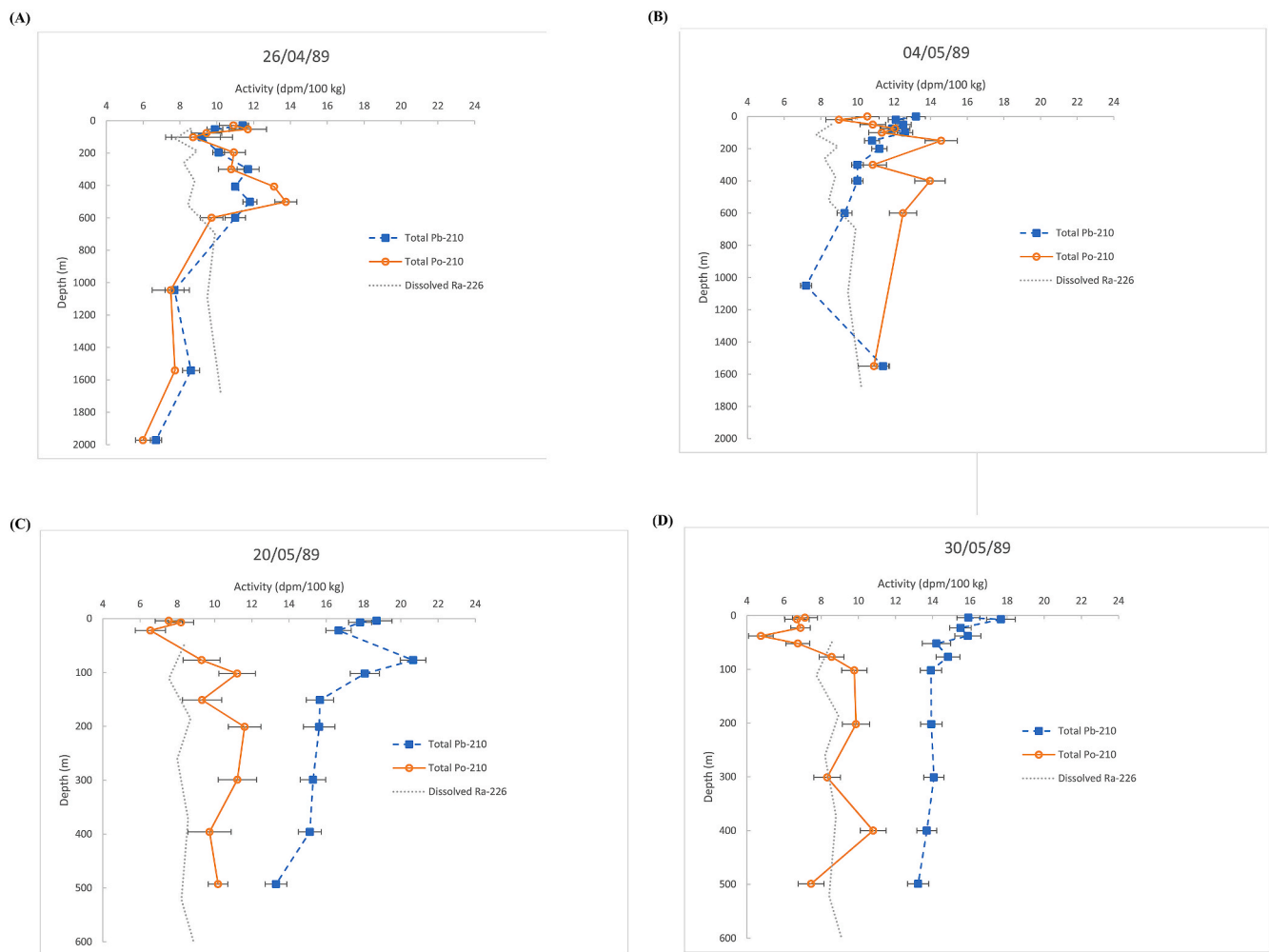
(A)

(B)

(C)

(D)

Fig. 2. A–D: Depth profiles of total ^{210}Po and ^{210}Pb at the NABE time-series site. Dissolved ^{226}Ra is from Le Roy et al. (2018). Errors are derived from 1σ counting uncertainty.

Table 3
Time-series station inventories of radionuclides integrated to 150 and 300 m and associated ^{210}Po deficits and SS fluxes.

Date	Depth (m)	^{226}Ra inventory (10^3 dpm m^{-2})	^{210}Po$_t$ inventory (10^3 dpm m^{-2})	^{210}Pb$_t$ inventory (10^3 dpm m^{-2})	^{210}Po deficit (10^3 dpm m^{-2})	SS P_{Po} (dpm m^{-2} d^{-1})	NSS[a] P_{Po} (dpm m^{-2} d^{-1})
26 April	150	12.7 ± 0.3	14.9 ± 1.1	15.0 ± 1.3	0.1 ± 1.7	0.5 ± 8.5	
	300	25.3 ± 0.4	31.2 ± 1.3	30.9 ± 1.5	-0.2 ± 2.0	-1.2 ± 12.0	
4 May	150	12.7 ± 0.3	17.2 ± 0.5	18.2 ± 0.3	1.0 ± 0.6	5.0 ± 3.0	-288
	300	25.3 ± 0.4	36.8 ± 0.6	34.9 ± 0.6	-1.9 ± 0.8	-9.5 ± 4.0	
20 May	150	12.7 ± 0.3	13.5 ± 0.7	27.1 ± 0.5	13.6 ± 0.9	68.2 ± 4.5	
	300	25.3 ± 0.4	26.7 ± 1.1	50.4 ± 0.9	20.2 ± 1.4	101.5 ± 7.0	
30 May	150	12.7 ± 0.3	12.2 ± 0.5	22.2 ± 0.4	10.0 ± 0.6	50.2 ± 3.0	194
	300	25.3 ± 0.4	26.2 ± 1.0	43.1 ± 0.8	16.9 ± 1.3	84.8 ± 6.5	

[a] NSS = Non-steady state ^{210}Po fluxes (eqn. (6)) calculated at 150 m for the 26 April – 5 May and 20 May – 30 May profiles.

similar pattern is seen in more recent GEOTRACES data from 47°N, 20°W, based on samples collected on 1 June 2014 (Le Roy et al., 2018) (Fig. 2 and Supplemental Fig. S3). The ^{226}Ra inventory over 150 m is 12.5×10^3 dpm/m^2 (Le Roy et al., 2018). ^{210}Pb inventories in the upper 150m are slightly in excess of that of ^{226}Ra on 26 April [$15.0 \pm 1.3 \times 10^3$ dpm/m^2], increase to $18.2 \pm 0.3 \times 10^3$ dpm/m^2 on 4 May, and then nearly double on the 20 and 30 May samplings [$27.1 \pm 0.5 \times 10^3$ and $22.4 \pm 0.4 \times 10^3$ dpm/m^2, respectively; Fig. 3 and Table 3]. The most noticeable increase is observed between 4 May and 20 May (Table 3). As noted above, sampling stations on 20 and 30 May after the leg change were almost three degrees of longitude to the east of those sampled on 26 April and 4 May (Fig. 1A–C), based on drifting of free-floating buoys

that designated the NABE site and eddy reports based on satellite altimetry data. Sampling was still within the "Small" eddy, but it is possible that different water masses were sampled at the NABE site on the first leg and the second leg as the eddy field evolved and the eddies interacted. The fact that the ^{210}Pb activities and inventories in the upper 300 m were significantly greater than those of ^{226}Ra (Table 3) implies that the source of the ^{210}Pb was atmospheric. Indeed, a large storm occurred on ~19–20 May, briefly interrupting sampling. The storm could have deposited ^{210}Pb and increased the inventories. However, the increase in inventories extends deeper in the water column than would have been likely after a storm event. We consider that evolution of the eddy field is a more likely explanation for the difference in the ^{210}Pb
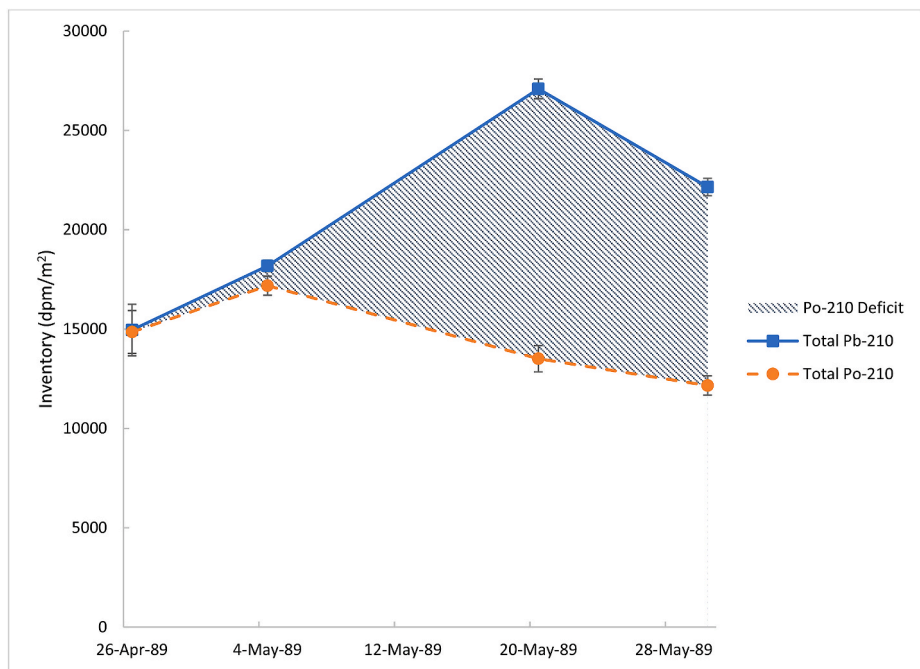
Fig. 3. Inventories of ^{210}Pb and [210]Po at 150 m during the time-series with [210]Po deficit shaded. Errors derived from propagated 1σ counting uncertainties.

Table 4
Transit station inventories of [210]Po and [210]Pb (to 150 and 300 m) and associated [210]Po deficits and SS fluxes.

Date	Depth (m)	[210]Po$_t$ inventory (10^3 dpm m^{-2})	[210]Pb$_t$ inventory (10^3 dpm m^{-2})	[210]Po deficit (10^3 dpm m^{-2})	SS P_{Po} (dpm m^{-2} day^{-1})
20 April	150	14.4 ± 0.2	17.3 ± 0.3	2.9 ± 0.4	14.7 ± 2.0
	300	28.0 ± 0.5	31.7 ± 1.0	3.7 ± 1.1	18.7 ± 5.6
22 April	150	14.8 ± 0.3	18.1 ± 0.6	3.3 ± 0.7	16.6 ± 3.5
	300	29.4 ± 0.4	35.0 ± 0.7	5.6 ± 0.8	27.9 ± 4.0
10 May	150	19.3 ± 0.7	19.5 ± 0.5	0.2 ± 0.9	0.9 ± 4.0
	300	38.1 ± 1.1	36.9 ± 0.7	-1.3 ± 1.3	-6.4 ± 6.4

profiles and inventories.

4.3. Dynamic [210]Pb-[210]Po disequilibrium

On 26 April, the mixed layer was over 100 m deep, but by 4 May, it was only ~20 m deep (Lochte et al., 1993; Fig. 4). Sometime between these two dates, stratification was established, and this is believed to be the start of the bloom, as seen by a concurrent loss of nutrients from surface water (Slagle and Heimerdinger, 1991, Fig. 5A). These assumptions are supported by the [210]Po and ^{210}Pb data, which show that the total [210]Po/^{210}Pb activity ratio in the near-surface water is essentially in equilibrium in late April but becomes much lower by late May. A similar trend is seen in the inventories of [210]Po and ^{210}Pb in the upper 150 m and 300 m (Tables 1, 4; Fig. 3).

Profiles of total [210]Po and [210]Pb (Fig. 2) depict a [210]Po deficit developing in the upper ~500–600 m by the 20 May profile. All four profiles in the time-series are similar in that they have a [210]Po minimum located near the bottom of the mixed layer (20–100 m), but there are substantial differences between the profiles. The 26 April "pre-bloom" profile shows the two radionuclides in near-equilibrium for almost all depths (Fig. 2A). The 4 May "beginning bloom" profile shows a small [210]Po deficit in the upper 100 m, but a [210]Po excess in the subsurface layer starting at 100 m before reaching equilibrium with ^{210}Pb in the sample taken a 1550 m (Table 1; Fig. 2B). The 20 and 30 May profiles (Fig. 2C and D) depict a water column deficient in [210]Po to at least 500 m. Even considering the possibility that the first two profiles sampled different water masses than the second two, the pattern of nutrients in

surface water (Fig. 4A) and in depth profiles taken virtually concurrent with the [210]Po/^{210}Pb sampling (Buesseler et al., 1992) indicate that sampling was proceeding over the development of a bloom. Taken together, the [210]Po and ^{210}Pb profiles indicate a lack of [210]Po export from the surface early in the bloom, but strong export later in the bloom. We posit that a large [210]Po deficit was not yet established on the first two dates because, while the bloom was in its beginning stage, there was not yet enough time for the [210]Po-containing particles to aggregate and sink, removing the [210]Po. Indeed, there was substantial particulate (>0.4 μm) [210]Po in the early stages of the bloom (Table 1; Fig. 5B), indicating uptake of polonium onto particles. Evidently the particles were either non-sinking or very slowly sinking. Aggregation and sinking later in the bloom produced a [210]Po deficit.

The profiles at the transit stations north of the NABE site (Supplemental Figs. S1A and B) show that there was an established [210]Po deficit on 20 and 22 April before sampling began at the NABE site (Table 2). This suggests earlier initiation of a bloom north of the NABE site. In contrast, there was no significant [210]Po deficit on 10 May at the transit station (41°5.8′N 23°1.8′W) south of the NABE site, while the bloom was clearly propagating at the NABE site. These observations are consistent with remote sensing of chlorophyll fluorescence of the NABE study site (Figure 16 in Robinson et al., 1993) which show high fluorescence within the cyclonic eddy where the NABE time-series stations were taken, and low fluorescence south of it.
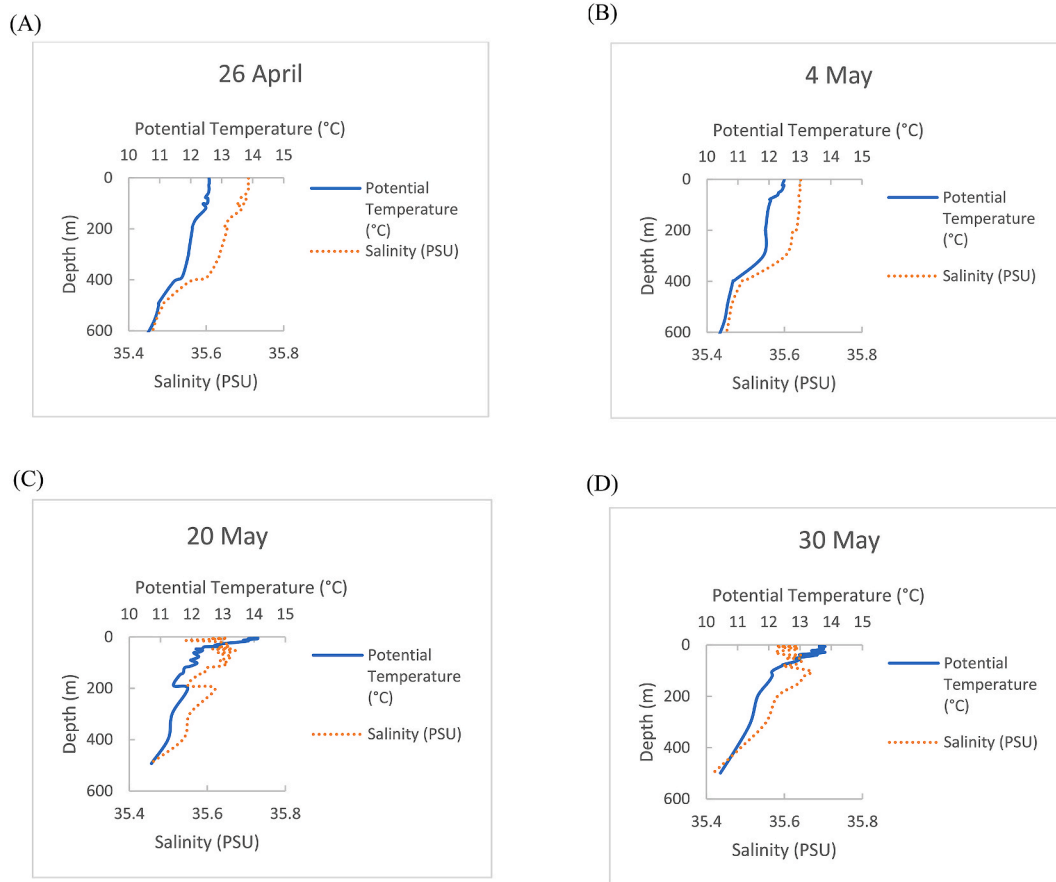
Fig. 4. Hydrographic data for the NABE site on dates sampled for [210]Po and [210]Pb. (A) 26/04/89; (B) 04/05/89; (C) 20/05/89; (D) 30/05/89. The surface mixed layer shoaled from ~100 m on 26 April to ~~10 m on 30 May.

4.4. Calculation of [210]Po fluxes

The change in the activities of dissolved and particulate [210]Po can be represented, respectively, as:

$$\frac{\partial A_{Po}^d}{\partial t} = A_{Pb} \times \lambda_{Po} - A_{Po}^d \times \lambda_{Po} - J_{Po} + V \tag{1}$$

$$\frac{\partial A_{Po}^p}{\partial t} = J_{Po} - A_{Po}^p \times \lambda_{Po} - P_{Po} + V \tag{2}$$

where A_{Pb}, A_{Po}^d and A_{Po}^p are the inventories (dpm/m^2) of total ^{210}Pb, and dissolved and particulate [210]Po respectively, λ_{Po} is the decay constant of [210]Po, J_{Po} is the rate of uptake of dissolved [210]Po onto particles, P_{Po} is the rate of removal (sinking) of particulate [210]Po and V is the advective and eddy diffusive input or output of [210]Po. We neglect the influence of any atmospheric flux on the Po profiles because atmospheric inputs of [210]Po are small (Baskaran, 2011). If steady state is assumed, $\frac{\partial A_{Po}^d}{\partial t} = 0$ and $\frac{\partial A_{Po}^p}{\partial t} = 0$, and advective and diffusive input or output of [210]Po is considered negligible, the equations condense to:

$$P_{Po} = \lambda_{Po}(A_{Pb} - A_{Po}) \tag{3}$$

where A_{Pb} and A_{Po} are the inventories of total ^{210}Pb and [210]Po (particulate + dissolved).

We determined steady-state (SS) [210]Po fluxes through 150 m and 300 m for each sampling date (Table 3 for the time-series stations; Table 4 for the transit stations). The calculations show significant [210]Po fluxes at the two transit stations taken on route to the NABE site (Table 4), but essentially no significant [210]Po flux from the upper 150 m at the time of first sampling at the NABE site (26 April; Table 3). Fluxes

at the NABE site increase with time, with a significant increase between the 4 May and 20 May profiles (Table 3). The steady-state [210]Po flux decreases slightly from 20 May to 30 May. No significant [210]Po flux was evident at the station taken on 10 May on route from the NABE site during the leg change (Table 4). The steady-state [210]Po export fluxes at 150 m for 20 and 30 May are generally in agreement those calculated with a steady-state approximation by Rigaud et al. (2015) in the upper 100 m of open ocean stations in the North Atlantic in autumn (63–68 dpm m^{-2} day^{-1}), where export was high. However, our SS [210]Po fluxes are generally much higher than those calculated by Tang et al. (2019) at the [234]Th equilibrium depth (~100 m) in nearly the same location (47°N, 20°W) in June 2014 (3.5 ± 1.8 dpm m^{-2} day^{-1}) (See Supplemental Fig. S3 for their measured [210]Po and ^{210}Pb activities). There are many possible explanations for this difference, but most likely, the bloom occurred at a different time or was of a smaller magnitude in 2014, lowering the deficit or allowing regrowth of [210]Po towards equilibrium.

These steady-state calculations ignore the fact that a bloom was occurring and that both the [210]Po and ^{210}Pb profiles and inventories were changing over the ~1 month of sampling. (Figs. 2 and 3). They also ignore advective fluxes. Sampling was in a cyclonic eddy and upwelling may have introduced [210]Po to the upper 150 m. Tang et al. (2019) argue that including vertical advection into the [210]Po flux equation is crucial since these terms can be of the same magnitude as the SS [210]Po flux calculated without them. Using the maximum recorded upwelling rate during this study (~0.5 m/d; Robinson et al., 1993), we can estimate the maximum contribution of vertical advection to the [210]Po flux, following the approach of Tang et al. (2019):

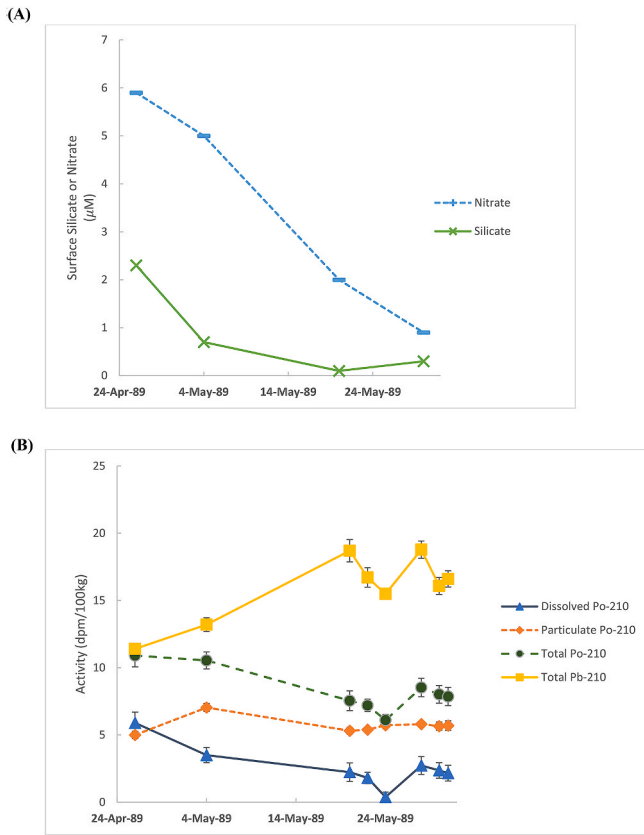$$F_w = w_{20}\left(A_{Po}^2 - A_{Po}^1\right) \tag{4}$$

Fig. 5. (A) Surface water nutrient concentrations (Slagle and Heimerdinger, 1991) and (B) Total ^{210}Pb and dissolved, particulate and total ^{210}Po in surface water at the NABE site (~46°N 20°W). Errors are derived from 1σ counting uncertainty.

where F_w is the Po flux due to upwelling at depth z (integration depth; here 150 m), w_{20} is the average vertical velocity between depths z and z + 20m (0.5 m/d), A_{Po}^1 is the averaged total ^{210}Po activity between depths 0 – z, and A_{Po}^2 is the total ^{210}Po activity at z + 20m (or the next deepest sample depth). This calculation yielded an F_w of 3.7 dpm m^{-2} d^{-1} on 26 April, 6.8 dpm m^{-2} d^{-1} on 4 May, 14.6 dpm m^{-2} day^{-1} on 20 May, and 13.3 dpm m^{-2} day^{-1} on 30 May. These values are greater than the steady state sinking flux of ^{210}Po calculated from the deficit on 26 April and 4 May, and are ~21% and 26% of the fluxes on 20 May and 30 May, respectively. The temporal pattern of increasing deficit and sinking flux of ^{210}Po is preserved even if these advective fluxes are taken into account. However, we do not have enough observations of vertical advection rates in the eddy(ies) sampled during NABE to validate these estimations and so neglect them in the following discussion.

We incorporate non-steady state into the calculation of the ^{210}Po fluxes using the approach of Friedrich and Rutgers van der Loeff (2002):

$$P_{Pb} = \lambda_{Pb} \left[\frac{A_{Ra}\left(1 - e^{-\lambda_{Pb}t}\right) + A_{Pb_1}e^{-\lambda_{Pb}t} + \frac{I_{Pb}}{\lambda_{Pb}}\left(1 - e^{-\lambda_{Pb}t}\right) - A_{Pb_2}}{\left(1 - e^{-\lambda_{Pb}t}\right)} \right] \tag{5}$$

where all terms are as defined in eqns. (1)–(3), and I_{Pb} is the atmospheric deposition of ^{210}Pb, (27.4 dpm m^{-2} d^{-1}, based on the 40–50°N latitudinal range tabulated by Baskaran, 2011), the subscripts *1* and *2* represent two successive profiles of ^{210}Po and ^{210}Pb and t is the time between the profiles. A_{Ra} is the inventory of ^{226}Ra for 150 m. As noted above, ^{226}Ra was not measured during the NABE cruise, so we use the ^{226}Ra profile from Le Roy et al. (2018) from nearly the same location (47°N, 20°W) to calculate the ^{226}Ra inventory. Moreover, because of the large change in ^{210}Pb inventory and 15-day gap between the two legs, we calculate NSS ^{210}Po fluxes only for the 26 April – 5 May and 20 May – 30 May samplings.

The ^{210}Po fluxes calculated with this NSS approximation are negative (−288 dpm m^{-2} d^{-1}) for the 26 April - 4 May interval, and increase substantially to 194 dpm m^{-2} d^{-1} in the 20 to 30 May interval (Table 3). For the 20 May – 30 May interval, they are ~2–4 times greater than those calculated using the steady state approach. We note that the increase in ^{210}Po flux from 4 to 20 May is produced principally from the increases in ^{210}Pb inventory, rather than a decrease in the ^{210}Po inventory (Table 3; Fig. 3). This reinforces the notion that the water mass sampled on 20 and 30 May was one with a different ^{210}Pb input and ^{210}Po scavenging history from that on 26 April and 4 May, even if sampling was still within the "Small" eddy. As noted above, the ^{210}Pb inventories in the upper 300 m at all times during the NABE sampling exceed those of ^{226}Ra (Table 3) and must have been ultimately derived from atmospheric input. Atmospheric ^{210}Pb deposition generally is accompanied with little ^{210}Po because of the relatively short residence time of atmospheric aerosols (Graustein and Turekian, 1996; Baskaran, 2011), and this may bias estimates of ^{210}Po scavenging and POC fluxes estimated from them toward higher values (Hayes et al., 2018; Tang et al., 2019). Without a clear knowledge of the history of atmospheric ^{210}Pb deposition at a sampling site, it is difficult to correct the ^{210}Po deficit for this effect.

4.5. POC/^{210}Po$_P$ ratios

The sinking flux of POC may be calculated from the ^{210}Po fluxes by multiplying the flux by the POC/^{210}Po ratio on the sinking particles, in a fashion analogous to the approach with the ^{234}Th-POC proxy (Buesseler et al., 1992; Stewart et al., 2007; Verdeny et al., 2009). The POC/^{210}Po (or POC/^{234}Th) ratio for this purpose is often taken as the ratio on large filtered particles (e.g. >51 or 70 μm) or on sediment trap material (e.g., Murray et al., 2005). More recently, Tang et al. (2017) and Tang and Stewart (2019) have argued that the POC/^{210}Po ratio on small particles (e.g. 1–51 μm) should be used. The slow sinking of such particles may be more consistent with the longer half-life of ^{210}Po and may dominate the ^{210}Po flux. For both the ^{234}Th- and ^{210}Po-POC flux proxies, the complication may be that the measurement of POC/^{234}Th or POC/^{210}Po on the day of sampling may not characterize the particles causing the radionuclide deficit.

During the NABE, particle-size fractionated ^{210}Po activities were not measured, and although sediment traps were deployed, ^{210}Po was not measured on those samples. However, we are able to compare the total particulate ^{210}Po (>0.4 μm) in the upper ~100 m with POC concentrations (>0.8 μm) measured over those depths (Slagle and Heimerdinger, 1991). Only the data from 20 to 30 May contained enough

$$P_{Po} = \lambda_{Po} \left\{ \frac{\frac{A_{Ra}\lambda_{Pb} + I_{Pb} - P_{Pb}}{\lambda_{Pb}}\left[\frac{\lambda_{Po}}{\lambda_{Po}-\lambda_{Pb}}\left(e^{-\lambda_{Po}t} - e^{-\lambda_{Pb}t}\right) + \left(1 - e^{-\lambda_{Po}t}\right)\right] + A_{Pb_1}\frac{\lambda_{Po}}{\lambda_{Po}-\lambda_{Pb}}\left(e^{-\lambda_{Pb}t} - e^{-\lambda_{Po}t}\right) + A_{Po_1}e^{-\lambda_{Po}t} - A_{Po_2}}{\left(1 - e^{-\lambda_{Po}t}\right)} \right\} \tag{6}$$

Table 5
Particulate ^{210}Po and POC data.

^{210}Po$_p$ Depth (m)	^{210}Po$_p$ (dpm/100kg)	Bottle POC Depth (m)	Bottle POC (μmol/L)	Average Depth (m)	POC/^{210}Po$_p$ (mmol/dpm)
20 May					
4	5.3	5	12.2	4.5	0.23
7	4.9	6	12.6	6.5	0.26
22	3.4	20	10.0	21.0	0.29
37	2.3	36	8.4	36.5	0.37
52	2.3	51	3.7	51.5	0.16
77	1.4	76.5	2.2	76.8	0.16
102	2.0	105.5	1.9	103.8	0.10
151	1.1	149	1.3	150.0	0.12
201	1.4	199	1.1	200.0	0.08
30 May					
7	6.1	6	13.5	6.5	0.22
23	4.1	23	13.8	23.0	0.34
38	2.0	39	10.2	38.5	0.51
52	1.5	53	4.3	52.5	0.29
77	1.1	81	2.2	79.0	0.20
102	1.0	103	1.2	102.5	0.12
202	1.0	201	1.2	201.5	0.12

matching data points (depths where both POC and ^{210}Po$_p$ concentrations were measured) to compare the profiles and calculate POC/^{210}Po$_p$ (Table 5). The POC/^{210}Po$_p$ profiles calculated in this manner for 20 May and 30 May are shown in Fig. 6A and B. Values increase with depth on both sampling dates to a maximum at ~37 m and then decrease. The maximum likely represents the subsurface chlorophyll maximum. The values at 150 m are similar on the two dates, 120 ($\pm$~25%) μmol/dpm, and these can be used to calculate the POC flux from the ^{210}Po deficit.

Previous studies have shown that the POC/^{210}Po ratio is greater on large filterable particles than on small filterable particles because small particles have a larger relative surface area, increasing adsorption of ^{210}Po (Stewart et al., 2011; Verdeny et al., 2009; Hayes et al., 2018; Tang et al., 2017, 2018). The NABE POC/^{210}Po ratios are close in value to North Atlantic in-situ pump observations on the small filterable fraction (290 $\pm$ 70 μmol/dpm; Rigaud et al., 2015) and of those measured in a sediment trap at ~100 m in the Mediterranean Sea, (66–309 μmol/dpm; Stewart et al., 2007). The NABE values are much lower than ratios from the large filterable (>70 μm) fraction during in-situ sampling at 100 m in the Mediterranean by Stewart et al. (2007), 987–1699 μmol/dpm, but closer to values from particles filtered in situ at 200 m (181–383 μmol/dpm). The NABE values are also similar to those calculated by Tang et al. (2019) near our study site at ~100 m (227–236 μmol/dpm; May–June 2014). The NABE POC/^{210}Po ratios also may differ somewhat from previous studies because of different filters used, as well as planktonic compositions, POC types (detritus, fresh phytoplankton, fecal pellets, etc.), and mixing regimes (Stewart et al., 2007; Rigaud et al., 2015).

4.6. Po-derived POC fluxes

Using the POC/^{210}Po ratio on filterable particles sampled on 20 and 30 May, we can calculate POC fluxes from the SS and NSS ^{210}Po fluxes determined for those dates (Table 3). Table 6 and Fig. 7 compares the Po-derived POC fluxes with sediment trap POC fluxes determined by Martin et al. (1993) on swimmer-picked material sampled by free-floating VERTEX-type traps at 150 m and NSS ^{234}Th-derived POC fluxes calculated by Buesseler et al. (1992) using the POC/^{234}Th ratios on particles collected from sediment traps as well as particles sampled by in-situ filtration (>1 μm). Steady state ^{234}Th fluxes were not calculated by Buesseler et al. (1992) or used to calculate POC fluxes from them, so we are unable to make comparisons with our steady state ^{210}Po-derived POC fluxes. Using the straightforward SS approximation based on the measured ^{210}Po deficit relative to ^{210}Pb, the ^{210}Po-derived
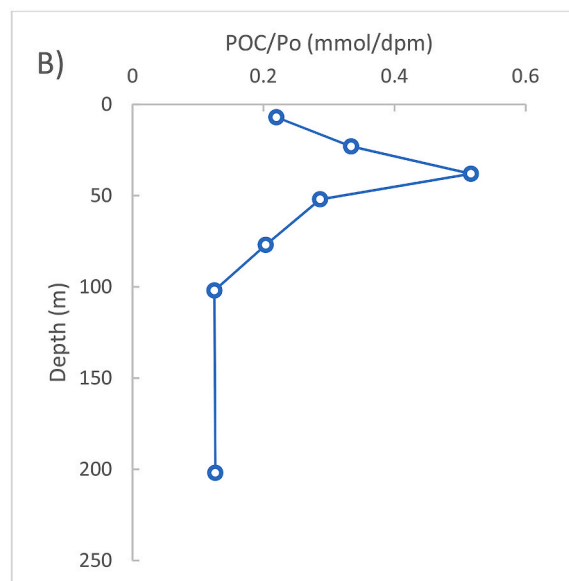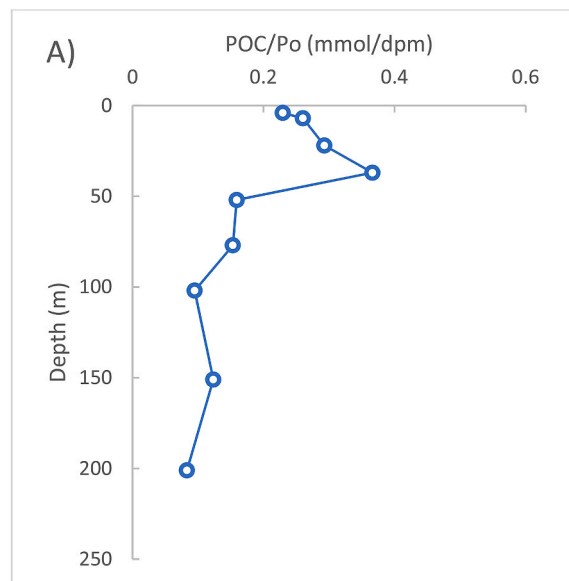

Fig. 6. Plots of Niskin bottle POC to Po_p ratio on particles of similar depths on A) 20 May and B) 30 May. The $\frac{POC}{^{210}Po_p}$ ratio at 150 m was 0.12 $\pm$ 0.02 mmol/dpm on 20 May and 0.12 $\pm$ 0.03 mmol/dpm on 30 May (interpolation for 30 May used 102 m and 202 m data; errors were propagated, with error on POC estimated at $\pm$10%). Bottle POC and Po_p samples were collected on the same day but on different casts, and were filtered differently (Bottle POC >0.7 μm; Po_p > 0.4 μm).

POC fluxes at 150 m are 8.5 and 6.3 mmol m^{-2} day^{-1} on 20 May and 30 May respectively. These are much lower than the NSS ^{234}Th-derived POC fluxes but very comparable to the sediment trap POC fluxes (Table 6, Fig. 7). The NSS ^{210}Po-POC flux is only calculated for the 20–30 May interval because POC/^{210}Po$_p$ ratios are based on sampling on those two dates. Taking the POC/^{210}Po$_p$ ratio for the two days (120 μmol/dpm), the NSS ^{210}Po-POC flux is 23.3 mmol m^{-2} day^{-1} at 150m. This is less than the NSS ^{234}Th-POC for the same interval, but within a factor of ~2 of the sediment trap POC flux (11.3 mmol m^{-2} day^{-1}; Martin et al., 1993). Thus, despite the uncertainties in the history of ^{210}Pb supply and scavenging at the NABE at the sampling site, the ^{210}Po-POC flux proxy produces fluxes that are comparable to POC fluxes

Table 6
NABE POC fluxes.

Date	Depth (m)	Sediment trap POC flux (mmol m^{-2} d^{-1})[a]	NSS ^{234}Th-POC flux (mmol m^{-2} d^{-1})[b]	NSS ^{210}Po-POC Flux (mmol m^{-2} d^{-1})[c]	SS ^{210}Po-POC Flux (mmol m^{-2} d^{-1})[d]
20 May – 30 May	150	11.6	37.3–45.0	23.3	–
20 May	150	–	–	–	8.2 ± 1.5
30 May	150	–	–	–	6.0 ± 1.6

[a] From Martin et al. (1993).

[b] From Buesseler et al. (1992). Based on NSS modeling of ^{234}Th profiles on May 19 and May 30. Low value was calculated using POC/^{234}Th ratio from sediment traps, high value was calculated using the ratio on filtered particles.

[c] Average of POC/^{210}Po ratio for May 20 and May 30 was used to calculate ^{210}Po-POC fluxes for 5/20–5/30.

[d] POC/^{210}Po ratio for May 20 was used to calculate 5/20 SS ^{210}Po-POC flux and ratio for May 30 was used to calculate 5/30 SS ^{210}Po-POC flux; errors were estimated based on errors in particulate ^{210}Po and POC.

measured in traps and those determined using ^{234}Th.

4.7. Links between the phytoplankton community and Po scavenging

During the sampling period of the NABE, it appeared that the phytoplankton community was controlled from the bottom up. Primary production was underutilized by grazing, and nutrient depletion throughout the study had pronounced effects on the phytoplankton community composition and abundance (Sieracki et al., 1993). Interestingly, Sieracki et al. (1993) postulated that the sequence of plankton succession they observed suggested that sampling occurred in different water masses, consistent with our observation of the increase in ^{210}Pb between the first and second legs of NABE. In terms of nutrients, silicate was the first nutrient to become depleted in surface water, from ~2 μM on 26 April to ~0.5 μM on 4 May and remained low for the remainder of the study (Fig. 5A; Chipman et al., 1993). Nitrate was slower to decrease, from ~6 μM on 26 April to ~0.5 μM on 30 May (Fig. 5A; Chipman et al., 1993). The early silicate depletion likely caused a change in the dominant microflora from diatoms to nanoflagellates late in the bloom (Sieracki et al., 1993). Generally, diatoms sink faster than nanoflagellates. In particular, nutrient-depleted diatoms can sink as fast as 70 m/day (Gemmell et al., 2016), while nanoflagellates typically do not sink faster than 1 m/day (Peperzak et al., 2003), so diatoms are potentially much greater contributors to both ^{210}Po and POC flux. Sieracki et al. (1993) conclude that the diatom bloom lasted two weeks

after 26 April (ending 10 May), then declined by four-fold and was replaced by phytoflagellates. Smetacek (1985) reported that nutrient depletion results in increased diatom mucus production, which in turn causes sinking aggregates to form. Additionally, Alldredge and Gotschalk (1989) directly observed the flocculation and sinking of diatoms in the presence of significant nitrate and hypothesized that this was caused by a depletion of silicate. As noted above (section 4.3), there was substantial particulate ^{210}Po early in the bloom sampling but no net ^{210}Po deficit relative to ^{210}Pb (Table 1) in the samplings on 26 April and 4 May (Table 3). Deficits became large on the 20 and 30 May samplings. This pattern is consistent with ^{210}Po uptake onto diatoms as they bloomed (26 April to 10 May; Sieracki et al., 1993), followed by diatom flocculation and sinking as silicate became depleted (Fig. 5).

During the senescence of diatoms, mucopolysaccharides are produced, mostly in the form of chitin microfibrils and gelatinous threads. Polysaccharides have been shown to strongly bond Th, decreasing the ratio of POC/^{234}Th found in particles in sediment traps (Quigley et al., 2002). Indeed, large amounts of this type of detritus (1/3 of all particulate carbon) were found in the water column near the end of the diatom bloom (20 May) but were not present on 30 May (Sieracki et al., 1993). This is consistent with lower POC/^{234}Th ratios during the 4–20 May interval compared with the 20–30 May interval in traps at 35m, 75m, 150m, and 300m (Buesseler et al., 1992). This indicated the end of what was probably a short pulse of sinking diatoms beginning sometime after 4 May and sinking below 300m or being otherwise removed sometime
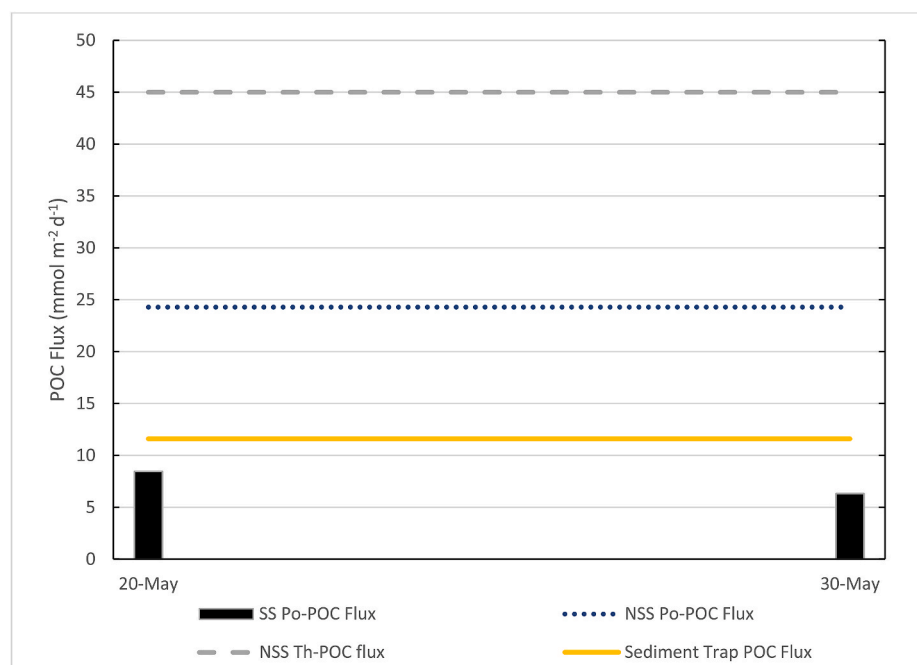

Fig. 7. POC flux estimated using different methods during the NABE. Steady-state (SS) Po-POC fluxes are based on the ^{210}Po deficiency integrated to 150 m on the indicated date (20 and 30 May) and the POC/Po$_p$ ratio at 150 m (see Fig. 4). Non-steady state (NSS) Po-derived POC fluxes are calculated as described in text and refer to the non-steady state flux between the two sampling dates. Non-steady state (NSS) ^{234}Th-derived POC flux (using POC/Th on filterable particles) and sediment trap POC flux at 150 m are from Buesseler et al. (1992) and Martin et al. (1993), respectively.

before 30 May. Our data on the particulate [210]Po/^{210}Pb activity ratios support this view in that they are high (3–24) in the photic zone early in the development of the bloom on 4 May (Table 1), but <5 on 20 and 30 May later in the bloom (Table 1). Thus the pattern of bloom development observed by Sieracki et al. (1993) is consistent with our observation of substantial particulate [210]Po in the upper ~100 m during late April to early May, yet little [210]Po deficit (Tables 1 and 3; Fig. 2A and B). Aggregation and sinking of diatoms as silicate was depleted could have produced the substantial deficits seen on 20 and 30 May (Tables 1 and 3; Fig. 2C and D). Particulate [210]Po observed during the 20 and 30 May samplings (Table 1) may have represented uptake on late-bloom, slowly sinking nanoflagellates.

Primary production between 26 April – 4 May was measured by Knudson et al. (1989) by in vitro ^{14}C incubation. The 24-h incubations estimated ~75 mmol C m^{-2} d^{-1} on 26 April and 4 May with a maximum of ~100 mmol C m^{-2} d^{-1} on 30 April. The maximum was most likely caused by the shoaling of the mixed layer from spring warming (Fig. 4), but POC flux was probably low during this time because older, aggregating and sinking organic matter was not yet present. Production from 18 to 30 May was measured by Martin et al. (1993), also with a 24-h ^{14}C incubation using trace metal-clean techniques, and values increased only from ~98 to ~105 mmol C m^{-2} d^{-1}. These production numbers by themselves would not suggest much change in [210]Po export over time, so the lower [210]Po fluxes on 30 May compared with 20 May do seem consistent with a change in biological community composition.

Cyanobacteria abundance was low on 26 April, slightly higher on 4 May, decreased on 10 May, before increasing back to 4 May levels by 20 May, and then sharply increasing on 30 May (Sieracki et al., 1993). Cyanobacteria have been proposed as a means of increasing the [210]Po deficit by efficiently assimilating [210]Po (as an analogue of sulfur) and rather than sinking, transferring it to higher trophic levels via grazing by nekton (Kim, 2001). Loss of [210]Po from the photic zone would then not be via export of sinking POC. Although this idea was postulated to explain an unexpected deficiency in oligotrophic regions of the ocean, it is possible that increasing cyanobacteria concentrations during the NABE created a [210]Po deficit that was not related to POC export. Thus, the phytoplankton community structure was not the only factor influencing the [210]Po-POC fluxes; bacterial consumption and zooplankton grazing also may have had a significant effect.

4.8. Bacteria and zooplankton grazing influences

It is widely assumed that the slope of a regression of POC versus chlorophyll-a in the euphotic zone represents carbon from photosynthesis, and the intercept represents detrital and zooplankton carbon (Banse, 1997). During the NABE, Dam et al. (1993) produced a regression with slope 79.2 μgC/μg Chl-a and intercept 31.2 μgC/L (n = 150; r^2 = 0.61; P < 0.01). This method estimated detrital and zooplankton carbon as 28% of the total carbon, a significant amount. Therefore, it is important to consider the zooplankton community in contextualizing our Po-derived POC flux estimates. The zooplankton stock increased threefold from 26 April to 30 May (Dam et al., 1993), and microzooplankton (sum of flagellates and ciliates) represented 30% of biomass on 20 May and 19% on 30 May (Sieracki et al., 1993). Microzooplankton were important grazers in late May (no data exist for late April - early May), consuming 32% of the standing stock of phytoplankton (Verity et al., 1993). However, they are a kind of intermediate in the POC export process, as neither they nor their fecal pellets sink very fast and so this compartment of POC is mostly either transferred up the trophic ladder or recycled by bacteria. Mesozooplankton may consume these microzooplankton, and it is estimated that 50% of their diet was other zooplankton (or detritus), with 50% being herbivory (Dam et al., 1993). Dam et al. (1993) measured very low mesozooplankton grazing rates of a few percent of phytoplankton standing stock, but Lenz et al. (1993) measured mesozooplankton grazing rates of 13% of standing stock for the same study period and site. This difference resulted most

likely from methodological differences but remains unresolved. As noted above, grazing may lead to loss of [210]Po that is not associated with sinking POC because the assimilation efficiency of Po from food is high, Indeed, Stewart and Fisher (2003) give an estimate of 40% assimilation efficiency, depending on the predator and prey species. As noted above, this effect may be a source of error resulting in an overestimate of POC fluxes calculated with the [210]Pb-[210]Po flux method, as Kim (2001) concluded. Mesozooplankton fecal pellets contributed <5% of POC export during the NABE (Dam et al., 1993), with microzooplankton fecal pellets conceivably a lower fraction. However, mesozooplankton defecation may have repackaged small, non-sinking phytoplankton into sinking fecal pellets that would have a significant effect on the POC export, as well as delivery of nutrients below the euphotic zone (Dam et al., 1993).

Bacterioplankton are a major part of the ocean carbon cycle, as they metabolize both POC and DOC. During the NABE, bacterioplankton made up a relatively small amount of the carbon stock (20–30% of POC above 50m and more below), but they have short turnover rates of about 0.3 day, so they are responsible for a large share of the carbon cycling (Ducklow et al., 1993). Bacterioplankton production accounted for 15–80% of the concurrent primary production, with peaks occurring on overcast days when photosynthesis was low, for about 30% of POC above 50m and more below, with an increasing trend from 10 May to 30 May (no data before 10 May) (Ducklow et al., 1993). Bacterial biomass increased five-fold from 26 April to 30 May, suggesting heavier recycling later in the bloom. Bacterivore activity was not consistent or significant at the NABE site (Ducklow et al., 1993), so their production was most likely recycled, as bacteria do not sink unless attached to larger ballasted particles. Therefore, the increasing abundance of bacteria was probably a hindrance to POC export as they are well known agents of carbon recycling in the layer just below the euphotic zone. In the euphotic zone, bacteria may compete with phytoplankton for nutrients (Kirchman et al., 1993; Ducklow et al., 1993). The rapid recycling of organic matter by bacteria is likely also to be associated with a rapid recycling of [210]Po, since microbial degradation of POM involves a rapid loss of proteins (Taylor, 1995). This process may help explain the lower [210]Po deficit on 30 May compared with 20 May, supported by the surface decrease in dissolved [210]Po and increase in particulate [210]Po after 20 May (Fig. 5).

5. Summary and conclusions

This study has enabled a test of the utility of disequilibrium between [210]Po and its grandparent ^{210}Pb as an indicator of scavenging and POC flux over the course of a spring bloom in the North Atlantic. Sampling was conducted in a small cyclonic eddy that was located near two larger eddies. Over the approximately 5-week occupation of the site (26 April to 30 May), [210]Po decreased from near-equilibrium with ^{210}Pb to displaying substantial deficits in the upper few hundred meters. [210]Pb inventories in the upper water column were in excess of those of [226]Ra, indicating input of ^{210}Pb from atmospheric deposition. [210]Pb inventories also displayed non-steady state conditions, increasing by ~50% in profiles sampled on the second leg relative to those on the first leg of the cruise. The source of the increased ^{210}Pb was predominately atmospheric because it was in excess of [226]Ra, and we hypothesize that evolution of the eddy field and possible interaction with nearby eddies resulted in somewhat different water masses being sampled. Although the two intervals of time sampled during this study might not represent the same water mass, they do represent different stages of a bloom, as ^{210}Pb/[210]Po disequilibrium was not established in the first interval but did occur during the second interval.

Non-steady state calculations of the export of [210]Po from the upper water column, taking into account non-steady state in ^{210}Pb, show higher fluxes during the 20 May to 30 May interval than the 26 April to 4 May interval. This is consistent with independent observations of the biological regime of the bloom, in that, although production was high

early in the bloom, export was low until nutrients were depleted and phytoplankton senesced, coagulated, and sank. POC data (>0.7 μm) available for 20 and 30 May, together with particulate ^{210}Po (>0.4 μm), permit calculation of the POC/^{210}Po ratios and the sinking flux of POC. At 150 m, the often-applied steady-state approach to the ^{210}Po deficit yields POC fluxes at 150 m that are quite comparable with floating trap fluxes during the same time interval - 8.2 mmol m^{-2} d^{-1} (20 May) and 6.0 mmol m^{-2} d^{-1} (30 May) vs 11.6 mmol m^{-2} d^{-1} (sediment trap; Martin et al., 1993). The non-steady state ^{210}Po-derived POC flux for the interval 20–30 May, 23.3 mmol m^{-2} day^{-1}, is comparable, but less than the NSS ^{234}Th-derived POC flux for the same interval (37.3–45.0 mmol m^{-2} day^{-1}; Buesseler et al., 1992). Non-steady state POC fluxes for both radionuclide pairs (Th/U and Po/Pb) give a POC flux greater than the sediment trap POC flux, and more research is required to reconcile the radionuclide proxies with each other and with traps. We conclude that ^{210}Po/^{210}Pb disequilibrium can be a useful proxy for POC export from the upper water column, especially if time series measurements of both radionuclides are available. However, it is possible that single occupations of stations may produce ^{210}Po and ^{210}Pb profiles that overestimate the ^{210}Po flux caused by sinking particles, depending on the history of atmospheric ^{210}Pb input or the possibility that Po is assimilated and transferred to higher trophic levels.

Declaration of competing interest

The authors declare that they have no known competing financial interests or personal relationships that could have appeared to influence the work reported in this paper.

Acknowledgements

Appendix A. Supplementary data

Supplementary data to this article can be found online at https://doi.org/10.1016/j.dsr.2020.103339.

References

Alldredge, A.L., Gotschalk, C.C., 1989. Direct observations of the mass flocculation of diatom blooms: characteristics, settling velocities and formation of diatom aggregates. *Deep Sea Research Part A*. Oceanograph. Res. Paper. 36 (2), 159–171. https://doi.org/10.1016/0198-0149(89)90131-3.

Bacon, M.P., Belastock, R.A., Tecotzky, M., Turekian, K.K., Spencer, D.W., 1988. Lead-210 and polonium-210 in ocean water profiles of the continental shelf and slope south of New England. Continent. Shelf Res. 8 (5), 841–853. https://doi.org/10.1016/0278-4343(88)90079-9.

Bacon, M.P., Spencer, D.W., Brewer, P.G., 1976. ^{210}Pb/^{226}Ra and ^{210}Po/^{210}Pb disequilibria in seawater and suspended particulate matter. Earth Planet Sci. Lett. 32 (2), 277–296. https://doi.org/10.1016/0012-821X(76)90068-6.

Banse, K., 1997. Determining the carbon-to-chlorophyll ratio of natural phytoplankton. Marine Biol. 41, 199–212. https://doi.org/10.1007/BF00394907.

Baskaran, M., 2011. Po-210 and Pb-210 as atmospheric tracers and global atmospheric Pb-210 fallout: a Review. J. Environ. Radioact. 102 (5), 500–513. https://doi.org/10.1016/j.jenvrad.2010.10.007.

Bhat, S.G., Krishnaswamy, S., Lal, D., Rama, Moore, W.S., 1968. ^{234}Th/^{238}U ratios in the ocean. Earth Planet Sci. Lett. 5, 483–491. https://doi.org/10.1016/S0012-821X(68)80083-4.

Broecker, W.S., Goddard, J., Sarmiento, J.L., 1976. The distribution of ^{226}Ra in the Atlantic Ocean. Earth Planet Sci. Lett. 32 (2), 220–235. https://doi.org/10.1016/0012-821X(76)90063-7.

Buesseler, K.O., Bacon, M.P., Cochran, J.K., Livingston, H.D., 1992. Carbon and nitrogen export during the JGOFS North Atlantic bloom experiment estimated from ^{234}Th: ^{238}U disequilibria. *Deep sea research Part A*. Oceanograph. Res. Paper. 39 (7), 1115–1137. https://doi.org/10.1016/0198-0149(92)90060-7.

Chen, J.H., Lawrence Edwards, R., Wasserburg, G.J., 1986. ^{238}U,^{234}U and^{232}Th in seawater. Earth Planet Sci. Lett. 80 (3), 241–251. https://doi.org/10.1016/0012-821X(86)90108-1.

Cherry, R.D., Heyraud, M., 1981. Polonium-210 content of marine shrimp: variation with biological and environmental factors. Marine Biol. 65 (2), 165–175. https://doi.org/10.1007/BF00397082.

Chipman, D.W., Marra, J., Takahashi, T., 1993. Primary production at 47°N and 20°W in the North Atlantic Ocean: a comparison between the 14C incubation method and the mixed layer carbon budget. Deep Sea Res. Part II Top. Stud. Oceanogr. 40 (1), 151–169. https://doi.org/10.1016/0967-0645(93)90011-B.

Chung, Y., Finkel, R., Bacon, M.P., Cochran, J.K., Krishnaswami, S., 1983. Intercomparison of ^{210}Pb measurements at GEOSECS stations in the northeast Pacific. Earth Planet Sci. Lett. 65, 393–405.

Cochran, J.K., Bacon, M.P., Krishnaswami, S., Turekian, K.K., 1983. ^{210}Po and ^{210}Pb distributions in the central and eastern Indian Ocean. Earth Planet Sci. Lett. 65 (2), 433–452. https://doi.org/10.1016/0012-821X(83)90180-2.

Cochran, J.K., Masqué, P., 2003. Short-lived U/Th series radionuclides in the ocean: tracers for scavenging rates, export fluxes and particle dynamics. Rev. Mineral. Geochem. 52 (1), 461–492. https://doi.org/10.2113/0520461.

Dam, H.G., Miller, C.A., Jonasdottir, S.H., 1993. The trophic role of mesozooplankton at 47°N, 20°W during the North Atlantic bloom experiment. Deep Sea Res. Part II Top. Stud. Oceanogr. 40 (1), 197–212. https://doi.org/10.1016/0967-0645(93)90013-D.

Ducklow, H.W., Harris, R.P., 1993. Introduction to the JGOFS North Atlantic bloom experiment. Deep Sea Res. Part II Top. Stud. Oceanogr. 40 (1), 1–8. https://doi.org/10.1016/0967-0645(93)90003-6.

Ducklow, H.W., Kirchman, D.L., Quinby, H.L., Carlson, C.A., Dam, H.G., 1993. Stocks and dynamics of bacterioplankton carbon during the spring bloom in the eastern North Atlantic Ocean. Deep Sea Res. Part II Top. Stud. Oceanogr. 40 (1), 245–263. https://doi.org/10.1016/0967-0645(93)90016-G.

Endrizzi, F., Rao, L., 2014. Chemical speciation of uranium(VI) in marine environments: complexation of calcium and magnesium ions with [(UO$_2$)(CO$_3$)^3]$^{4-}$ and the effect on the extraction of uranium from seawater. Chem. Eur J. 20 (44), 14499–14506. https://doi.org/10.1002/chem.201403262.

Fleer, A.P., Bacon, M.P., 1984. Determination of ^{210}Pb and ^{210}Po in seawater and marine particulate matter. Nucl. Instrum. Methods Phys. Res. 223 (2), 243–249. https://doi.org/10.1016/0167-5087(84)90655-0.

Flynn, W.W., 1968. The determination of low levels of polonium-210 in environmental materials. Anal. Chim. Acta 43, 221–227. https://doi.org/10.1016/S0003-2670(00)89210-7.

Friedrich, J., Rutgers van der Loeff, M.M., 2002. A two-tracer (^{210}Po–^{234}Th) approach to distinguish organic carbon and biogenic silica export flux in the Antarctic Circumpolar Current. Deep Sea Res. Oceanogr. Res. Pap. 49 (1), 101–120. https://doi.org/10.1016/S0967-0637(01)00045-0.

Gemmell, B.J., Oh, G., Buskey, E.J., Villareal, T.A., 2016. Dynamic sinking behaviour in marine phytoplankton: rapid changes in buoyancy may aid in nutrient uptake. Proc. Biol. Sci. 283 (1840).

Graustein, W.C., Turekian, K.K., 1996. ^{7}Be and ^{210}Pb Indicate an upper troposphere source for elevated ozone in the summertime subtropical free troposphere of the eastern North Atlantic. Geophys. Res. Lett. 23 (5), 539–542. https://doi.org/10.1029/96GL00304.

Hayes, C., Black, E.E., Anderson, R.F., Baskaran, M., Buesseler, K.O., Charette, M.A., Cheng, H., Cochran, D.C., Edwards, R.L., Fitzgerald, P., Lam, P.J., Lu, Y., Morris, S. O., Ohnemus, D.C., Pavia, F.J., Stewart, G., Tang, Y., 2018. Flux of particulate elements in the North Atlantic Ocean constrained by multiple radionuclides. Global Biogeochem. Cycles 32 (12), 1738–1758. https://doi.org/10.1029/2018GB005994.

Hedges, J.I., Baldock, J.A., Gélinas, Y., Lee, C., Peterson, M., Wakeham, S.G., 2001. Evidence for non-selective preservation of organic matter in sinking marine particles. Nature 409, 801. https://doi.org/10.1038/35057247.

IAEA, 1985. Sediment Kd's and Concentration Factors for Radionuclides in the Marine Environment. International Atomic Energy Agency, Vienna.

Kim, G., 2001. Large deficiency of polonium in the oligotrophic ocean's interior. Earth Planet Sci. Lett. 192 (1), 15–21. https://doi.org/10.1016/S0012-821X(01)00431-9.

Kim, G., Church, T.M., 2001. Seasonal biogeochemical fluxes of ^{234}Th and ^{210}Po in the Upper Sargasso Sea: influence from atmospheric iron deposition. Global Biogeochem. Cycles 15 (3), 651–661. https://doi.org/10.1029/2000GB001313.

Kirchman, D.L., Keel, R.G., Simon, M., Welschmeyer, N.A., 1993. Biomass and production of heterotrophic bacterioplankton in the oceanic subarctic Pacific. Deep Sea Res. Oceanogr. Res. Pap. 40 (5), 967–988. https://doi.org/10.1016/0967-0637(93)90084-G.

Knudson, C., Chamberlin, W.S., Marra, J., 1989. Primary production and irradiance data for US JGOFS (Leg 2) ATLANTIS II (Cruise 119-4). L-DGO Tech. Rep. LDGO- 89, 4.

Le Roy, E., Sanial, V., Charette, M.A., van Beek, P., Lacan, F., Jacquet, S.H.M., Henderson, P.B., Souhaut, M., Garcia-Ibanez, M.I., Jeandel, C., Perez, F.F., Sarthou, G., 2018. The ^{226}Ra–Ba relationship in the North Atlantic during GEOTRACES-GA01. Biogeosciences 15 (9), 3027–3048. https://doi.org/10.5194/bg-15-3027-2018.

Lenz, J., Morales, A., Gunkel, J., 1993. Mesozooplankton standing stock during the North Atlantic spring bloom study in 1989 and its potential grazing pressure on phytoplankton: a comparison between low, medium and high latitudes. Deep Sea Res. Part II Top. Stud. Oceanogr. 40 (1), 559–572. https://doi.org/10.1016/0967-0645(93)90032-L.

Lochte, K., Ducklow, H.W., Fasham, M.J.R., Stienen, C., 1993. Plankton succession and carbon cycling at 47°N 20°W during the JGOFS North Atlantic bloom experiment. Deep Sea Res. Part II Top. Stud. Oceanogr. 40 (1), 91–114. https://doi.org/10.1016/0967-0645(93)90008-B.

Martin, J.H., Fitzwater, S.E., Gordon, R.M., Hunter, C.N., Tanner, S.J., 1993. Iron, primary production and carbon-nitrogen flux studies during the JGOFS North Atlantic bloom experiment. Deep Sea Res. Part II Top. Stud. Oceanogr. 40 (1), 115–134. https://doi.org/10.1016/0967-0645(93)90009-C.

Murray, J.W., Paul, B., Dunne, J.P., Chapin, T., 2005. ^{234}Th, ^{210}Pb, ^{210}Po and stable Pb in the central equatorial Pacific: tracers for paryicle cycling. Deep-Sea Res. I 52, 2109–2139.

Nozaki, Y., Zhang, J., Takeda, A., 1996. ^{210}Pb and ^{210}Po in the equatorial Pacific and the Bering Sea: the effects of biological productivity and boundary scavenging. Deep Sea Res. Part II Top. Stud. Oceanogr. 44 (9), 2203–2220. https://doi.org/10.1016/S0967-0645(97)00024-6.

Peperzak, L., Colijn, F., Koeman, R., Gieskes, W.W.C., Joordens, J.C.A., 2003. Phytoplankton sinking rates in the Rhine region of freshwater influence. J. Plankton Res. 25 (4), 365–383. https://doi.org/10.1093/plankt/25.4.365.

Pfannkuche, O., 1993. Benthic response to the sedimentation of particulate organic matter at the BIOTRANS station, 47°N, 20°W. Deep-Sea Res. Part II Top. Stud. Oceanogr. 40 (1/2), 135–150.

Quigley, M.S., Santschi, P.H., Hung, C.-C., Guo, L., Honeyman, B.D., 2002. Importance of acid polysaccharides for ^{234}Th complexation to marine organic matter. Limnol. Oceanogr. 47 (2), 367–377. https://doi.org/10.4319/lo.2002.47.2.0367.

Rigaud, S., Stewart, G., Baskaran, M., Marsan, D., Church, T., 2015. ^{210}Po and ^{210}Pb distribution, dissolved-particulate exchange rates, and particulate export along the North Atlantic US GEOTRACES GA03 section. Deep Sea Res. Part II Top. Stud. Oceanogr. 116, 60–78. https://doi.org/10.1016/j.dsr2.2014.11.003.

Robinson, A.R., McGillicuddy, D.J., Calman, J., Ducklow, H.W., Fasham, M.J.R., Hoge, F. E., Leslie, W.G., McCarthy, J.J., Podewski, S., Porter, G., Saure, G., Yoder, J.A., 1993. Mesoscale and upper ocean variabilities during the 1989 JGOFS bloom study. Deep Sea Res. Part II Top. Stud. Oceanogr. 40 (1), 9–35. https://doi.org/10.1016/0967-0645(93)90004-7.

Sieracki, M.E., Verity, P.G., Stoecker, D.K., 1993. Plankton community response to sequential silicate and nitrate depletion during the 1989 North Atlantic spring bloom. Deep Sea Res. Part II Top. Stud. Oceanogr. 40 (1), 213–225. https://doi.org/10.1016/0967-0645(93)90014-E.

Slagle, R., Heimerdinger, G., 1991. North Atlantic Bloom Experiment, April-July 1989 Process Study Data Report P-L. NODC/U S JGOFS Data Management Office, Woods Hole, MA, U S A.

Smetacek, V., 1985. Role of sinking in diatom life-history cycles: ecological, evolutionary and geological significance. Marine Biol. 84, 239. https://doi.org/10.1007/BF00392493.

Stewart, G., Cochran, J.K., Miquel, J.C., Masqué, P., Szlosek, J., Rodriguez y Baena, A.M., Fowler, S.W., Gasser, B., Hirschberg, D.J., 2007. Comparing POC export from ^{234}Th/^{238}U and ^{210}Po/^{210}Pb disequilibria with estimates from sediment traps in the northwest Mediterranean. Deep Sea Res. Oceanogr. Res. Pap. 54 (9), 1549–1570. https://doi.org/10.1016/j.dsr.2007.06.005.

Stewart, G.M., Fisher, N.S., 2003. Bioaccumulation of polonium-210 in marine copepods. Limnol. Oceanogr. 48 (5), 2011–2019. https://doi.org/10.4319/lo.2003.48.5.2011.

Stewart, G., Moran, S.B., Lomas, M.W., Kelly, R.P., 2011. Direct comparison of ^{210}Po, ^{234}Th and POC particle-size distributions and export fluxes at the Bermuda Atlantic Time-series Study (BATS) site. J. Environ. Radioact. 102 (5), 479–489. https://doi.org/10.1016/j.jenvrad.2010.09.011.

Tang, Y., Castrillejo, M., Roca-Martí, M., Masqué, P., Lemaitre, N., Stewart, G., 2018. Distributions of total and size-fractionated particulate 210Po and 210Pb activities along the North Atlantic GEOTRACES GA01 transect: GEOVIDE cruise. Biogeosciences 15 (17), 5437–5453. https://doi.org/10.5194/bg-15-5437-2018.

Tang, Y., Lemaitre, N., Castrillejo, M., Roca-Martí, M., Masqué, P., Stewart, G., 2019. The export flux of particulate organic carbon derived from ^{210}Po/^{210}Pb disequilibria along the North Atlantic GEOTRACES GA01 transect: GEOVIDE cruise. Biogeosciences 16 (2), 309–327. https://doi.org/10.5194/bg-16-309-2019.

Tang, Y., Stewart, G., Lam, P.J., Rigaud, S., Church, T., 2017. The influence of particle concentration and composition on the fractionation of ^{210}Po and ^{210}Pb along the North Atlantic GEOTRACES transect GA03. Deep Sea Res. Oceanogr. Res. Pap. 128, 42–54. https://doi.org/10.1016/j.dsr.2017.09.001.

Tang, Y., Stewart, G., 2019. The ^{210}Po/^{210}Pb method to calculate particle export: lessons learned from the results of three GEOTRACES transects. submitted for publication.

Taylor, G.T., 1995. Microbial degradation of sorbed and dissolved protein in seawater. Limnol. Oceanogr. 40 (5), 875–885. https://doi.org/10.4319/lo.1995.40.5.0875.

Verdeny, E., Masqué, P., Garcia-Orellana, J., Hanfland, C., Kirk Cochran, J., Stewart, G. M., 2009. POC export from ocean surface waters by means of ^{234}Th/^{238}U and ^{210}Po/^{210}Pb disequilibria: a review of the use of two radiotracer pairs. Deep Sea Res. Part II Top. Stud. Oceanogr. 56 (18), 1502–1518. https://doi.org/10.1016/j.dsr2.2008.12.018.

Verdeny, E., Masqué, P., Maiti, K., Garcia-Orellana, J., Bruach, J.M., Mahaffey, C., Benitez-Nelson, C.R., 2008. Particle export within cyclonic Hawaiian lee eddies derived from ^{210}Pb–^{210}Po disequilibrium. Deep Sea Res. Part II Top. Stud. Oceanogr. 55 (10), 1461–1472. https://doi.org/10.1016/j.dsr2.2008.02.009.

Verity, P.G., Stoecker, D.K., Sieracki, M.E., Burkill, P.H., Edwards, E.S., Tronzo, C.R., 1993. Abundance, biomass and distribution of heterotrophic dinoflagellates during the North Atlantic spring bloom. Deep Sea Res. Part II Top. Stud. Oceanogr. 40 (1), 227–244. https://doi.org/10.1016/0967-0645(93)90015-F.